Shear-Sensitive Polymer Dispersed Liquid Crystal

Guo Shi Li

A thesis

Submitted in partial fulfillment of the

requirements for the degree of

Master of Science in Aeronautics and Astronautics

University of Washington

2012

Committee:

Dana Dabiri, Chair

Gamal Khalil

Program Authorized to Offer Degree:

Aeronautics and Astronautics

University of Washington

Abstract

Shear-Sensitive Polymer Dispersed Liquid Crystal

Guo Shi Li

Chair of the Supervisory Committee:

Dana Dabiri

Department of Aeronautics and Astronautics

Polymer dispersed liquid crystal has been developed as a shear stress sensor, showing a great signal-to-noise ratio with a high temporal bandwidth. Traditional shear sensing liquid crystal techniques are known to be irreversible processes under practical test conditions. The introduction of polymer into the liquid crystal gives the shear-sensor an additional temporal bandwidth that can be utilized for detecting unsteady flow phenomena. Exploiting a revolutionary dynamic birefringence detecting system known as "Milliview", a series of liquid crystal polymer combinations were tested in a wind tunnel apparatus. The signal strength and the reversibility of the tested combinations are summarized in this paper. The preliminary results showed promising potential in this new sensor system. It demonstrated the capability of the sensor in commercial wind tunnel applications. The dynamic range and the bandwidth of the sensor can be adjusted to fit different application needs. Few combinations presented qualities both in high dynamic range and in broad bandwidth, making them ideal broad purpose sensors.

Table of Contents

List of Figures

Acknowledgements

First and foremost, the author wishes to express his deepest gratitude to his family for their love and support. The author would like to express his most sincere appreciation to Professor Dana Dabiri, Professor Gamal Khalil and Professor Werner Kaminsky for their guidance and support throughout the course of his Master of Science degree. The author also thanks Dr John West of Kent **S**tate University for his advice on the project.

A special thank also gives to Kenneth Low for his dedicated assistance on the project. The author wishes to thank Viggo Hansen for his help on the project and the equipment donated. Thanks are also given to Alex Perez, Wei-Hsin Tien, Kristina Wang and Trenton West for their friendship and daily support. The author also wishes to thank for the technical support received from Aeronautics & Astronautics Engineering as well as Mechanical Engineering machine shops, namely, Dzung Tran, Dennis Peterson, Eamon McQuaide and Kevin Soderlund. The same kind of gratitude goes towards Robert Gordon.

,

Chapter 1. Introduction

Friction induced by air flowing over aerodynamic surfaces is a fundamental force that theoretical and experimental aerodynamicists aim to calculate and measure. This force, also known as shear stress, has traditionally been measured point-by-point across surfaces, a process that can be both expensive and time consuming. The resolution of the shear stress maps is dependent upon the number of points taken across the surface. To improve upon this technology, a novel method for obtaining high-resolution, 2-dimensional shear stress measurements over aerodynamic surfaces is proposed. The method is based upon dynamic birefringence measurements of a shear sensitive, liquid crystal coating. Promising to produce a robust, non-intrusive, and real-time shear stress measuring technique, this method can be utilized on any aerodynamic surface. In this chapter we will review some of the current methods for measuring shear stress and will provide a brief description for the proposed technique.

1.1 Shear stress measurement

Shear stress and pressure are the two predominant sources of force that act on any aerodynamic surface. While pressure acts normal to the surface, shear stress acts tangential to the surface and is a significant contributing factor to the drag force.

Shear stress measurements can be utilized as a means of studying and understanding skin friction. The development of a technique to measure shear stress is difficult due to the demanding requirements imposed upon the bandwidth and spatial resolution needed to measure the smallest eddy size present in the flow. Three technologies are available to accomplish the proposed tasks: microelectromechanical systems (MEMS), thin oil films, and liquid crystal coatings. A comprehensive review of shear stress measurement technologies developed is given in [5].

1.1.1 MEMS based technologies

Microelectromechanical system (MEMS) is a field that extends silicon-based integrated circuit (IC) microfabrication to the construction of miniature engineering systems [1]. These sensors can be categorized into two main groups: direct sensors and indirect sensors. Direct sensors include the typical flush mounted floating elements that

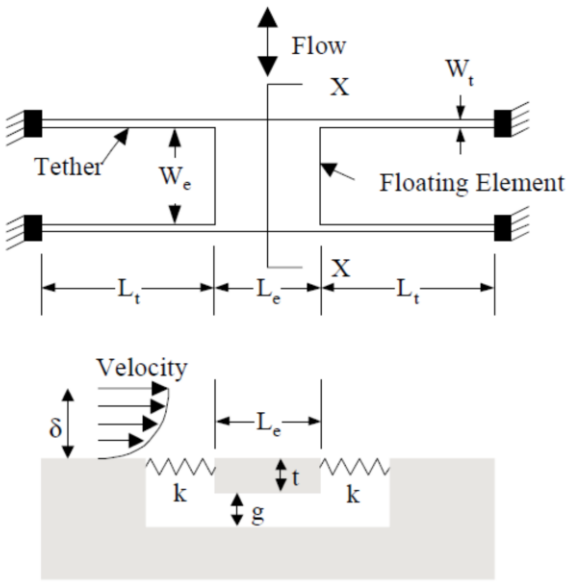

Figure 1.1 Schematic of a typical floating point. *Subscript t indicates tether dimension. Subscript e indicates element dimension. g is the height of the gap between the floating element and the substrate. t is the thickness of the element and the tether. The figure is adapted from Naughton and Sheplak [5].*

integrate force produced by the wall shear stresses. Direct sensors using floating element on a macro-scale have been extensively developed; however, due to constraints on dimensions, it is almost impossible for macro-scaled floating element sensor to achieve the dynamic bandwidth and spatial resolution that are needed to measure the shear stress in a turbulent boundary layer. This is because the dynamic bandwidth of the floating element is directly proportional to its natural frequency. A schematic of typical floating element design is shown in Fig. 1.1 [5]. The displacement Δ can be correlated to shear stress τ_w through Euler-Bernoulli beam theory as shown in Eq. (1)

$$\Delta \approx \tau_w \frac{A}{4Et}\left(\frac{L_t}{W_t}\right)^3\left(1+2\frac{L_tW_t}{L_eW_e}\right), \qquad (1)$$

where A is the area of the element exposed to the shear stress and E is the elastic modulus of the tether material. Assume the tether to element area ratio is close to zero, the spring constant of the tether can be estimated using Eq. (2)

$$k \approx \frac{\tau_w A}{\Delta} \approx 4Et\left(\frac{L_t}{W_t}\right)^{-3}. \qquad (2)$$

The dynamic bandwidth of the floating element can be estimated using the natural frequency of the device as shown in Eq. (3).

$$\omega_n = \sqrt{\frac{k}{m}} \approx \sqrt{\frac{1}{4E\rho L_eW_et^2}\left(\frac{L_t}{W_t}\right)^3}. \qquad (3)$$

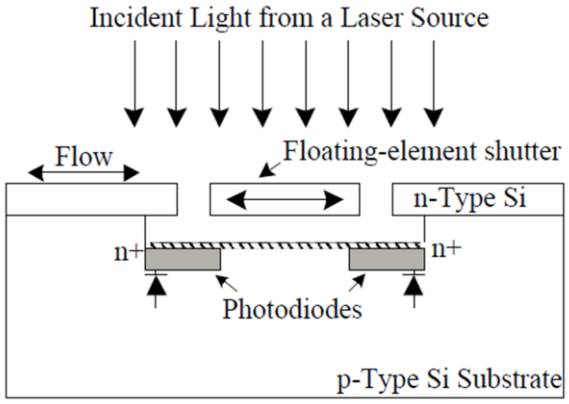

Figure 1.2 Schematic of the optical shutter design. *Integrated photodiodes are under different areas of exposure. This figure is adapted from Padmanabhan [6].*

Simple dimensional analysis using Eq. (3) can show that by reducing the size of a 1cm x 1 cm x 1mm floating element to 100 μm x 100 μm x 1 μm, the dynamic bandwidth can be improved at least five-orders of magnitude [5]. Realizing such benefits, Schmidt *et al*. [2], first exploited the micromachining technology by developing a polyimide/aluminum surface, and a differential capacitive technique to measure the movement of the floating element. It demonstrated the huge potential of MEMS, including a high dynamic bandwidth up to 10 kHz, large dynamic range of 0.01-1Pa, etc. However it has also shown to be problematic. Moisture variations changed the mechanical properties of the polyimide which led to mechanical sensitivity drift [5]. The technique is also prone to electromagnetic noise interference (EMI). Other methods, including piezoresistive based [3, 4], force-feedback capacitive based [7, 8], and optical shutter-based [9, 6, 10, 11], have then emerged to perfect this technology. Among these, the optical shutter-based sensors stand out as a new potential candidate for MEMS. Figure 1.2 illustrates the schematic of this design. It has a demonstrated maximum nonlinearity of 1% over a dynamic range spanning from 1.4mPa to 10Pa. It also possesses a verified bandwidth of up to 4 kHz, which has been qualitatively shown to exceed 10 kHz [11, 12]. Unlike the differential capacitive technique, it is also insensitive to environmental effects such as moisture and EMI. It is, however, sensitive to the position variation of the light source which is mounted separately. Though the advantages of direct MEMS compared to their macro scale counterparts are significant, they are not without limitations. Winter [13] summarizes these limitations as follows:

(1) The spatial resolution is constrained by the dynamic range of the sensor.

(2) Sensor packaging and installation caused errors.

(3) Pressure gradients caused measurement errors.

(4) Cross-axis sensitivity due to thermal expansion, vibration, and acceleration.

Indirect MEMS rely on empirical or theoretical correlations to relate the measured quantity to shear stress. Examples include thermal films [14, 15, 16] and laser Doppler measurement [17, 18] as well as the recently developed micro-pillars [19, 20]. Thermal films have recently surpassed the near-wall hot-wire method as they are guaranteed to be within the boundary layer and they are insensitive to the pitch angle of the flow. Thermal films operate on the similar principle to the near-wall hot-wire anemometer. As heat transfers away from the hot-film sensor, the resistance of hot-film changes according to the temperature variation. Since the variation of the heat transfer rate is mainly due to the convective heat transfer within the fluid, the signal caused by this resistance variation can be used to measure the wall shear stress. A widely used general scaling approximation of the relationship is that the Nusselt number of the sensor is proportional to the wall shear stress to the third power. This relationship has been used with the assumption that the thermal boundary layer generated by the hot-film is fully submerged under the boundary layer. In the review paper written by Haritonidis[21], this scaling relationship was shown to be valid only when the Peclet number is above 100. As one of the most developed shear stress measuring techniques, hot-films have shown promising results at various situations such as during transition, local separation, or shock oscillation [15]. One of the drawbacks of the hot-film sensors is the difficulty of obtaining a unique relationship between the heat transfer and the wall shear stress. This is due to the heat transfer being a function of a multitude of parameters such as substrate heat conduction and yaw angle of the flow. Haselbach *et al*. [15] have pointed out a trade-off relationship between the dynamic bandwidth and the sensitivity of the sensor based on the choice of substrate material. Higher thermal conductivity and diffusivity of the substrate material leads to an increase in the dynamic bandwidth of the sensor at the cost of reduced sensitivity of sensor. Elvery and Bremhost [14] did a detailed analysis of how the yaw angle of the flow affects the hot-film signal. Though they demonstrated a relationship between the yaw angle of the flow and the hot-film signal at a given speed, such a relationship would be only useful if the streamline information is known. Such parameter dependency results in the hot-film technology being useful only if it is calibrated ahead of time to the experimental conditions with a reference method and used in situations where the

streamline information is already known. Realizing this need for calibration, Chandrasekaran *et al*. [16] have developed a calibration technique that uses a known super-imposed sinusoidal shear stress over an established mean flow to calibrate the sensor. Acoustic plane wave excitation of a shear stress sensor allows for calibration up to a dynamic bandwidth of 20 kHz. The main source of error is caused by the temperature drift in the mean flow. Another noteworthy limitation of the technique is the spatial resolution of the sensors. In their analysis of in-line hot-film arrays, Haselbach *et al*. [15] have also pointed out that the measurement error increases asymptotically with decreased spacing of the sensors.

MEMS based on Laser Doppler Effect have also been developed recently and have shown promising results, such as a 99% accuracy up to $Re_x = 10^6$ [18]. However its main limitation at this time is the low near-wall seeding density, since only the seeds within the sub-viscous layer can be used to estimate wall shear stress. This limits the technology to measuring the unsteady behavior of the flow.

Micropillars are an emerging technology that has shown a huge potential. This technology optically measures the tip movement of micro-scale pillars that protrude into the viscous sub-layer of the flow. Große *et al*. [19, 20] have done extensive work deriving a correlation between the tip movement of the pillars due to the fluid bending force and the wall shear stress. In their derivation, a linear velocity profile within the sub-layer of the fluid is assumed. Based on this correlation, Micropillars can give a detailed shear-stress measurement of both magnitude and direction over a large area with sufficient spatial resolution. With current technology, Micropillars can be manufactured from a height range of 80 to 1000 μm and an aspect ratio of 15-25. This physical limitation sets the upper limit of the dynamic bandwidth of the sensors, which currently has been only measured up to 2050 Hz [19]. A 10-15% gain yield bandwidth is predicted due to improvements of the manufacturing technology. The lowest dynamic range limit is set by the noise level of measurement, which makes the current smallest detectable wall shear-stress to be about 10mPa [19]. Micropillars emerge as a promising technology because of their ability to measure both the magnitude as well as direction with a much better spatial resolution than other aforementioned MEMS based technologies. It does have a few

drawbacks, including a limited temporal resolution as well as the intrusive nature of the method. Even with a predicted 10-15% increase of dynamic bandwidth, a 2 kHz dynamic range cannot allow this technology to be competitive with other high temporal resolution technologies such as the optical shutter based MEMS. Since the current technology requires the sensors to be illuminated from underneath, models being measured have to be made of a transparent material; this leads to greater design and construction complexity. These disadvantages are likely to be improved with further work and development. They have also been developing a reflective illumination technique to improve the invasive nature of the method. Another disadvantage is due its small size and the optical measurement nature. In order to be able to see the individual pillar, the field of view must limited within a 6 cm x 6 cm area. This drawback limits its capability of being used on a bigger scale, such as wind tunnel applications.

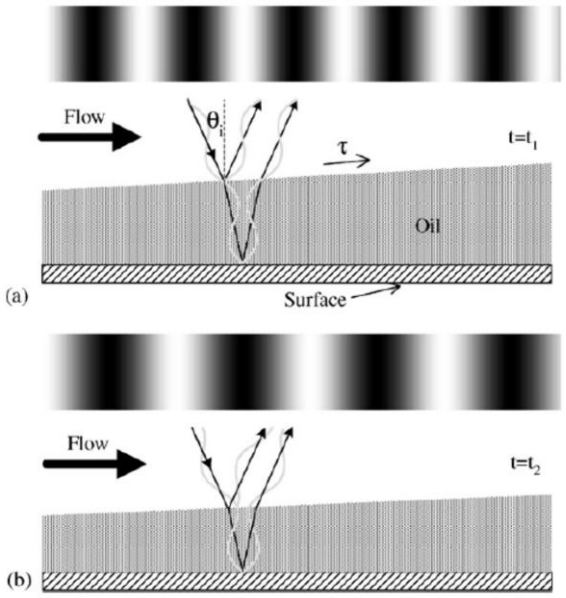

Figure 1.3 Interference pattern produced by Fizeau Interferomery. *(a) Fringe pattern at time $t = t_1$. (b) Fringe pattern at $t = t_2$. Light either constructively or destructively recombines to form the fringe pattern which changes according to the shear stress. The figure is adapted from Naughton and Sheplak [5].*

1.1.2 Thin oil film

Squire [22] first derived the thin-oil-film equation to prove that the oil-film technique that often is used in wind tunnels as a streamline visualization method actually indicates the streamline pattern. Squire found that oil followed surface streamlines except when separation happened; he also proved that oil film has little effect on the boundary layer. Tanner and Blows [23] first realized the potential of this theory to be utilized as a surface shear stress measurement technique. They simplified Squire's thin-oil-film equations to present a simpler correlation between thinning rate to surface shear

stress. They also decided to use interferometry as their method to measure the thickness of the oil film. This became the predominant technique for all oil film shear stress sensors. The principal of interferometry is illustrated in Fig. 1.3. When the incident light hits the thin oil film, part of the light reflects off the surface of the film while the rest of it is reflected from the substrate. The thickness of the film decides the phase delay between the two reflected light beams. This phase delay causes the reflected lights to either constructively or destructively combine together. This induces a fringe pattern that can be seen from the interferometry: the destructive part darkens while the constructive part lights up. This fringe pattern can be correlated back to the thickness of the film which in turn can be correlated back to shear stress based on Squire's thin-oil-film equation. Another major advancement of the technique occurred a decade later when Monson *et al*. [24, 25] at NASA Ames recognized that the thin-oil-film equation can be integrated, thus only one image by the end of the test would be sufficient to derive the mean shear stress. They also introduced a few surface techniques that can be used on normal wind tunnel data that will give a good fringe pattern. This along with Tanner and Kulkarni's [26] suggestion of using oil drops instead of a continuous oil-film have pushed thin-oil-film technology to where it is today. The current thin-oil-film technologies can be categorized into two groups: 1-D and 2-D. The 1-D technologies are based on the aforementioned techniques, using oil drops over a large area with only one image being taken after the test, are sufficient to determine both mean shear stress magnitude as well as direction. The simplicity of the technique, however, leads not only to a significant advantage but also to a considerable drawback. The single image by the end of test method basically neglected any transient behavior of the flow. This results in the technique being useful only for steady-state shear stress measurement. The 2-D technology is based on a discretized version of Squire's thin-oil-firm equation. It links the 2-D shear stress to the location and height of the oil-film. Unlike the 1-D method, this technique requires two images to be taken in order to calculate the mean shear stress in between the two instances. Since shear stress is only averaged between the two frames, temporal resolution is dramatically improved. The spatial resolution of the method, however, remains fairly low, since oil drops have to be separated by their streak distances. Thin oil films are also sensitive to environmental conditions such as temperature of the flow

which affects the viscosity of the oil. Dust and humidity of the flow can also destroy the fringe pattern.

1.1.3 Liquid crystal

Liquid crystal is a state of matter that is between solid and liquid. It behaves like liquid on macroscopic scale; however, it shows order in molecular arrangement on a microscopic scale. Normally liquid crystal molecules have a long rod shape, which gives them two unique refractive indices, one measured along the long axis of the rod and one measured perpendicular to it. The direction where the long axis points to is called director. Figure 1.4 shows some of the normal molecular arrangements that most liquid crystals can take at different temperatures. Due to the unique property of dynamic birefringence, liquid crystals are ideally suited to be utilized as a means of measuring shear stress. There are two major techniques in shear-sensitive liquid crystal: color based and intensity based. Chiral nematic liquid crystals are normally chosen in color based technique. In this state, liquid crystals form a helix structure where all liquid crystals in each layer share a common director that is parallel to the layer. These directors twist at different angles across different layers to form the helix pattern. If the vertical axis of the helix structure is parallel to the normal of the substrate then it is called the Grandjean state; otherwise it is called Focal Conic state. A change in selective reflection in light can happen either when liquid crystal changes from Focal Conic state to Grandjean state or when the pitch of the helix pattern changes. Both of these motions can be induced by shear stress. The change in selective reflection results in a change of color that is also dependent on viewing angle. Reda, *et al.* [27, 28, 29] at NASA Ames research center capitalized on this concept and demonstrated a shear stress measurement technique based on the color observation of the sample. Since color is a function of viewing angle,

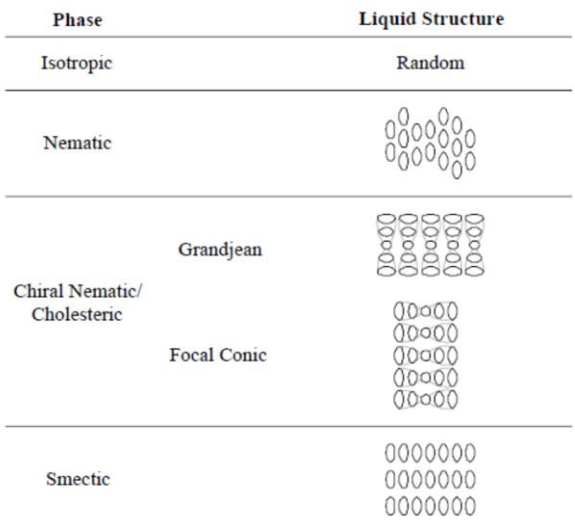

Figure 1.4 Sub-states of liquid crystal. *[5]*

multiple images at different viewing angles have to be used in order to establish a Gaussian distribution and find the true hue of the color. This limitation not only places a stringent requirement on the mounting angle of the cameras but also makes measurements on any curvilinear surface difficult to calibrate. Recently, however, Fujisawa *et al*. [30] demonstrated that by using only two cameras, they can acquire the shear stress measurement over a NACA 0018 airfoil. Another disadvantage of this technique is the complex data analysis. The biggest advantage of the liquid crystal technique is near infinite spatial resolution. Reda, *et al*. [32] also studied the temporal resolution of the liquid crystal, which they concluded to be on the order of 1 kHz. Unlike color based technique, intensity based technique normally uses nematic liquid crystal. In this state, order only presents in a common director in liquid crystal direction. No positional order exists in this state. This means it is more flexible then the chiral nematic state. Shorter response time, therefore, can be expected comparing to the chiral nematic state. When subjected to shear stress, the director of the liquid crystals aligns according to the magnitude and direction of the shear stress. This motion causes a corresponding change of birefringence value of liquid crystals. This change in birefringence value can be simply detected by placing the sample in between a pair of crossed linear polarizers. When the birefringence value is low, the crossed linear polarizers let a very small amount of light through. The intensity of the light passing through this sandwiched set starts increasing as the birefringence value increases. Buttsworth *et al*. [31] did a full-field-shear-stress-measurement based on this theory. However, a major disadvantage of both of these techniques is the temporal resolution. Even though the liquid crystal has a relatively small response time, the motion of the liquid crystal is irreversible. Theoretically, the resolution can be improved by comparing frame-to-frame changes of the sensor. However, since both techniques can only be calibrated under a steady flow, it is almost impossible at this stage to resolve the frame-to-frame change of shear stress.

1.2 Shear-Sensitive Polymer Dispersed Liquid Crystal

Shear-sensitive polymer dispersed liquid crystal (PDLC) was developed to overcome the aforementioned disadvantages of shear-sensitive liquid crystal techniques. First introduced by Parmar and Singh [33], shear-sensitive PDLC utilizes the structure rigidity provided by the polymer film to improve the temporal resolution of the sensor.

However, he didn't relate the signal to shear stress, nor did he study the reversibility of the PDLC. When the proper polymer is mixed with liquid crystals, liquid crystals form droplets within the polymer film. Nematic liquid crystal was normally chosen to make the PDLC sensor. As the second most disordered liquid crystal state next to the isotropic state, nematic liquid crystal, therefore, inherently has a low viscosity and a fast response time. All liquid crystals within one droplet share a common director. If there was no external aligning field when the film was cured, these directors across different droplets will point at random directions. As shown in Fig. 1.5 when subjected to a shear stress, these liquid crystal droplets elongate according to the shear stress. This motion causes the directors to align. The alignment of the nematic liquid crystal gives a coherent change in PDLC's birefringent value, which can be correlated back to the shear stress. If the polymer was chosen in such a way that the refractive index of the polymer matches the one of the refractive index of the liquid crystal, the birefringent value change from each droplet in the PDLC sensor is similar to that of the intensity based shear stress sensor. However, adding polymer into the film is not without complications. If the droplets' size is around one order of magnitude bigger than the visible light, the randomly initial alignment of the droplets induces a strong scattering effect. Since the birefringent value can only be optically determined, light transmission is critical for the birefringence measurement. This scattering effect can be improved through an initial alignment of the droplets' directors. Though it has not been tested within this study, the theoretical benefits of the initial alignment will be elaborated later in this paper. Another complication is the added temporal resolution dependency on the PDLC film's response time. The response time of the liquid crystal is no longer the sole determinant factor of the temporal resolution of the sensor. Instead it is dependent on the smallest response time between the liquid crystal and the PDLC film. The response time of the PDLC film can be estimated using the shear wave velocity of the PDLC film

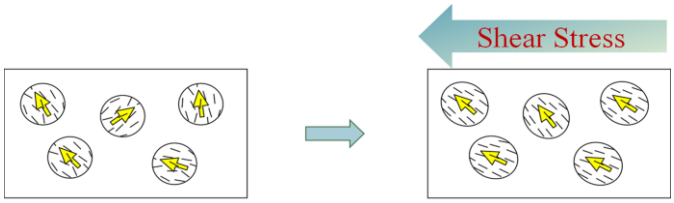

Figure 1.5 PDLC under shear stress. *Yellow arrows represent the directors of liquid crystals inside a droplet. The black lines inside circles represent the liquid crystal molecules. These directors align according to the shear stress.*

and the thickness of the film. The shear velocity defined in Eq. (4) describes how fast shear waves travels in the elastic material.

$$C_s = \sqrt{\frac{G}{\rho}}, \qquad (4)$$

where G and ρ are the shear modulus and the density of the material respectively. The response time of the PDLC film can then be estimated using the thickness of the film divided the shear velocity. Since the normal thickness of the PDLC film is on the order of 10 μm, this estimation shows that the PDLC film's response time is at least two orders of magnitude smaller than that of the response time of the liquid crystal. Therefore the temporal resolution of the PDLC sensor is determined by the liquid crystal's response time.

1.3 Imaging polarimetry system

As mentioned before, color based liquid crystals have to face the challenge of complex data analysis. Though intensity based liquid crystal's signal can be measured simply using a pair of crossed linear polarizers, this method doesn't take the full advantage of liquid crystal sensor, this because it can't obtain directional information. In an effort to improve upon this method, a better acquisition system that is easy to use and can provide detailed birefringent value and direction is in need. Glazer, Lewis and Kaminsky [34] first laid the foundation for the possibility of such a system. They presented a method utilizing circular polarized light as the light source. When circular polarized light passes through a birefringent media, each of the two refractive indices gives different phase retardations to the light. This phenomenon changes circular polarized light into elliptically polarized light, with the long and short axis proportional to the two distinct

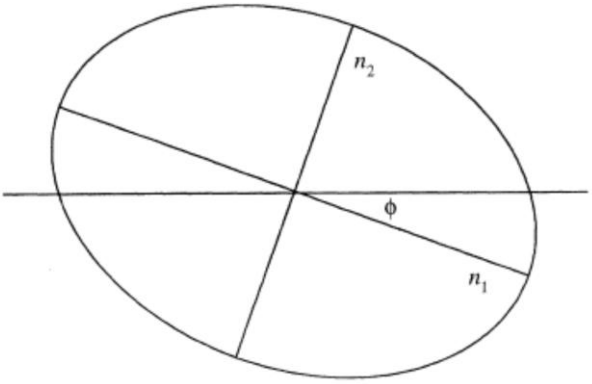

Figure 1.6 Elliptically polarized light. *ϕ is the extinction angle measured from the slow axis (larger refractive index) to the horizontal (with respect to the linear polarizer.)*

refractive indices. Thus, the birefringence can be determined by measuring the properties of the elliptically polarized light. This elliptically polarized light also contains directional information. Birefringent material inherently contains an extinction angle. If the material placed at the extinction angle no light would be able to pass through, since the two reflected lights lines up with the angles of the two crossed linear polarizers. This phenomenon occurs four times every rotation placed *π/2* apart. In elliptically polarized light, this extinction angle is shown in Fig. 1.6. It can be used to relate back to the direction of the shear stress, since this extinction angle describes the direction the ellipse is pointing to. Glazer, Lewis and Kaminsky [34] in their paper demonstrated a system using a rotating linear polarizer to detect the elliptically polarized light passed from the birefringent media sample. The key concept behind this technique is listed in Eq. (5) [34].

$$I = \frac{1}{2} I_0 [1 + sin2(\omega t - \phi) sin\delta]. \quad (5)$$

I_0 is the initial intensity of the circular polarized light and I is the intensity measured behind the rotating linear polarizer. The frequency of the rotating polarizer is ω and t is time. The phase shift δ is a value that can be used to correlate to the birefringence as shown in Eq. (6) [34].

$$\delta = \frac{\pi}{\lambda} \Delta n L. \quad (6)$$

λ is the wavelength of the light. Δn is the birefringence value and L is the thickness of the birefringent material. In the PDLC film the birefringence is only a function of the angle between the director of the droplet and the substrate normal as shown in Eq. (7) [36], if the polymer's refractive index is close to the refractive index of the liquid crystal measured along the long axis.

$$\Delta n \approx (n_e - n_o) sin^2\theta, \quad (7)$$

where n_e and n_o are the extraordinary and the ordinary refractive indices of the liquid crystal respectively. The angle between the liquid crystal director and the substrate normal is θ.

As can be seen by measuring the intensity of the elliptically polarized light passing through the rotating linear polarizer, both the birefringence and the direction can

be calculated. Kaminsky *et al*. [35] later improved this method by realizing that only four intensity values are enough to determine the birefringence and the extinction angle, if they can be taken simultaneously behind four differently aligned linear polarizers. This can be seen through changing the time dependent term ωt in Eq. (5) with a set of angles α_i at which the linear polarizers are placed at as shown in Eq. (8) [35].

$$I_i = \frac{1}{2} I_0 [1 + sin2(\alpha_i - \phi) sin\delta]. \quad (8)$$

Since α_i are the only variables, Eq. (7) can be linearized and expressed in form of Eq. (9) [35].

$$I_i = a_0 + a_1 sin2\alpha_i + a_2 cos2\alpha_i, \quad (9)$$

where a_0, a_1, and a_2 are coefficients that can be linked back to I_0, ϕ, and δ through the set of equations shown in Eq. (10) [35].

$$a_0 = \frac{1}{2} I_0,\ a_1 = \frac{1}{2} I_0 sin\delta cos\phi, a_2 = -\frac{1}{2} I_0 sin\delta sin\phi. \quad (10)$$

They also can be calculated using the intensity values measured as shown in Eq. (11) [35].

$$a_0 = \sum_{i=1}^{N} \frac{1}{N} I_i,\ a_1 = \sum_{i=1}^{N} \frac{2}{N} I_i sin2\alpha_i, a_2 = \sum_{i=1}^{N} \frac{2}{N} I_i cos2\alpha_i. \quad (11)$$

If these linear polarizers are set at angles 0^o, 45^o, 90^o and 135^o, Eq. (11) can be taken in forms of Eq. (12) [35].

$$a_0 = \sum_{i=1}^{N4} \frac{1}{N} I_i,\ a_1 = \sum_{i=1}^{4} \frac{2}{4} I_i sin2\alpha_i = \frac{1}{2}(I_2 - I_4), a_2 = \frac{1}{2}(I_1 - I_3). \quad (12)$$

The term $|sin\delta|$ which is a function of the birefringence Δn only and can be calculated using Eq. (13) [35].

$$|sin\delta| = \frac{1}{a_0} \sqrt{a_1^2 + a_2^2}. \quad (13)$$

The extinction angle, which contains the shear stress directional information, can be expressed as in Eq. (14) [35].

$$\phi = \frac{\pi}{2} + sgn(a_2)\frac{1}{2}arccos\left(\frac{-a_1}{\sqrt{a_1^2+a_2^2}}\right). \quad (14)$$

Based on this algorithm, Kaminsky *et al*. [35] then developed a real time birefringence and extinction angle measurement system called "MilliView". It utilizes an image-multiplexing device that has been developed by Optical Insights, LLC (Santa Fe, NM) that makes real-time birefringence and extinction measurements a reality. The device, known as Quad-View, is essentially a camera lens fitted with a 4-sided prism. This prism splits the sample image into four reflections that are mirrored back to a CCD camera. The resulting four simultaneous images are then focused on the surface of the camera as an array. The Quad- View is fitted with four linear polarizers set at the aforementioned angles thus eliminating the need for mechanical rotation. Figure 1.8 demonstrates the functional groups of the Quad-View system. This system, "MilliView", revolutionized intensity

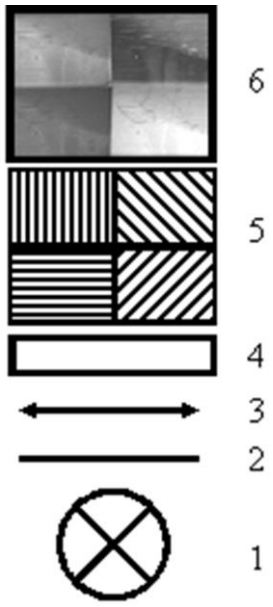

Figure 1.8 Optical components of "MilliView". *1. Light source; 2. Bandpass filter; 3. Circular polarizer; 4. Sample; 5. Quad View; 6. Color CCD camera.*

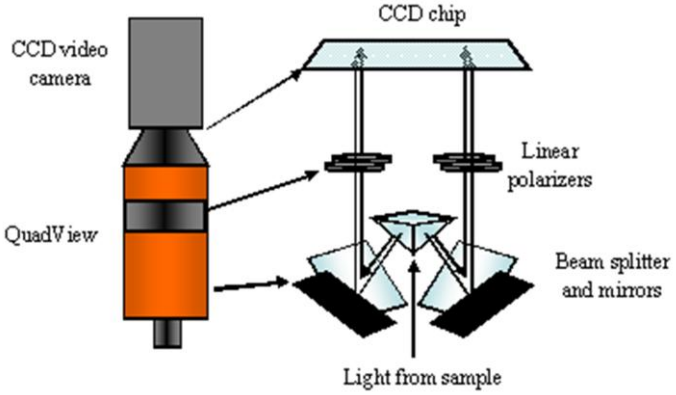

Figure 1.7 Functional Groups of Quad-View. *Light from the sample enters the prism and splits into four beams bouncing back from the mirrors before it goes through four differently aligned linear polarizers. Then the four intensity images go in to the CCD chip. Note: The linear polarizers must be adjusted such that the mirror effects are accounted for.*

based shear sensitive liquid crystal by producing real-time images that generate quantitative maps of sin (δ) and θ. The optical components of "MilliView" are shown in Fig. 1.7.

1.4 Objectives

The objectives of the current project comprise of the following points listed below.

1.4.1 Wind tunnel applicable

As most of the current shear-sensitive liquid crystal applications stay in the experimental stage, the object of this project is to push this technology one step closer to being utilized in a commercial set up. In order to achieve this object, a series of obstacles must be overcome. The light source and imaging system should stay outside the wind tunnel and must not move with respect to each other and to the tested model. This means the system must be able to overcome the vibrations of the wind tunnel and still capable of accurately measuring shear stress. It also must be insensitive to other parameters such as temperature, humidity, expansion of the window when the wind tunnel is running, and fine particulate matters.

1.4.2 Uniform and high signal-to-noise ratio

The PDLC sensor must not change the nature of the flow over the tested surface. This requires the PDLC film to be smooth. It also needs to be able to provide uniform results across the entire testing surface. Thus, the sensor will not need to be calibrated locally. In order to provide useful results, it also must have a sufficient signal-to-noise ratio. Only proper polymer and liquid crystal combinations can form good PDLC film. However, this process is complicated and depends on various variables. This means only through testing different combinations, the performance of the PDLC can be concluded. There is no existing theory to predict which combination would work well. Various application methods need to be tested as well, such as airbrushing, direct deposit, and spin coating.

1.4.3 Macro scale imaging with high resolution

In order to become feasible in wind tunnel application, the optical system needs to be able to provide a detailed 2-D shear stress map over a large testing surface. This puts

stringent requirements on the optical system. The light source must be strong enough to provide sufficient and uniform lighting across the testing surface. The imaging system must be able to zoom in a relatively large area with enough resolution to provide detailed information. Since the aforementioned Quad-view system spilts the incoming image into four identical images, each of these four images can only obtain at maximum one quarter of the intensity of the original image. The CCD chip's field of view is also reduced to one quarter of the original area at maximum. This puts even higher restrictions on the light source and the optical system.

Chapter 2. Experimental facilities, instrumentation and set up

2.1 Calibration facilities

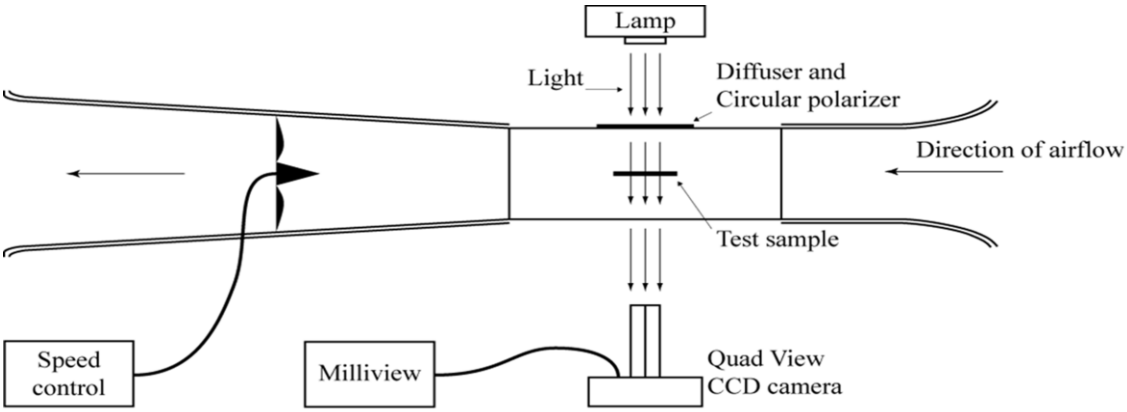

Figure 2.1 Experimental Apparatus. *Light from the light source passing through the diffuser and the circular polarizer becomes circular polarized. Then it passes though the sample enters the Quad-View system before it is captured by the CCD camera. CCD camera sends the collected image to be analyzed in the Milliview.*

Figure 2.1 illustrates the schematic of the experimental apparatus. The key component is a Jet Stream 500 wind tunnel. Using the measured wind speed from a Pitot tube inside the test chamber as feedback signal, Jet Stream 500 utilizes a proportional-integral-derivative (PID) controller to adjust the input power to the 1 hp AC motor providing user designated wind speed from 0 to 80 MPH. To avoid birefringence effect, all the transparent sides of the test chamber were sealed using annealed thick glass. The cross section of the test chamber is 5.25 inches by 5.25 inches square. The Pitot tube was adjusted to the side of the chamber to avoid the sample affected by the flow disturbance induced by the Pitot tube. A precision rotational stage was constructed to position the test plate inside the test chamber such that the tested aerodynamic surface can be set to an angle of attack ranging from -17^{o} to $+17^{o}$ in one degree steps. Detailed drawings of the test chamber can be found in Appendix A.

Light is provided by a Lumitex, Inc 2-Port Source powered by a 21V, 150W halogen lamp. The 150W halogen lamp provides more than sufficient lighting required for the back lighting scheme where the sample is in between the light source and the imaging system. Light coming from the light source first encounters a diffuser plate to

make the illumination more uniform across the testing area. A circular polarizer set is placed immediately after the diffuser. It consists of a linear polarizer and a quarter wave plate laminated together at an angle that is optimized for 570nm wavelength. The diffuser plate and the circular polarizer set is laminated together and placed on the side of the wind tunnel test chamber.

Current PDLC films are tested on 25 mm x 75 mm glass micro-slide substrate that is placed in the middle of the test chamber. On the other side of the wind tunnel, the imaging system consists of an adjustable lens, the Quad-View system, and a CCD camera that are secured together on the same frame structure which is also supporting the light source. This frame structure is also clamped on the test chamber using 6 C-Clamps. This set up makes sure that the light source, test sample, and the imaging system will have minimum movement relative to each other, despite the vibration caused by the running wind tunnel. The lens used in the imaging system is a Computar 1/2" 4-8mm Megapixel Lens with manual iris. The specification sheet of the lens is provided in Appendix B. The CCD camera used in this set up is a 3.0 mega pixel Am Scope MD 800 E color CCD camera. The "MilliView" software is installed on a computer that is connected to the CCD camera using a USB 2.0 cable.

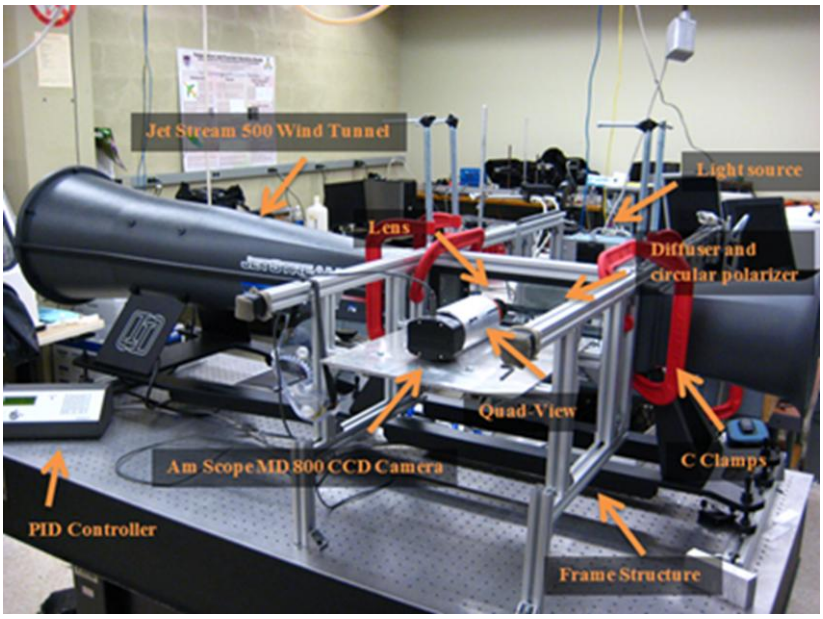

Figure 2.2 Calibration facilities. *Omitted details can be found in Fig. 2.3.*

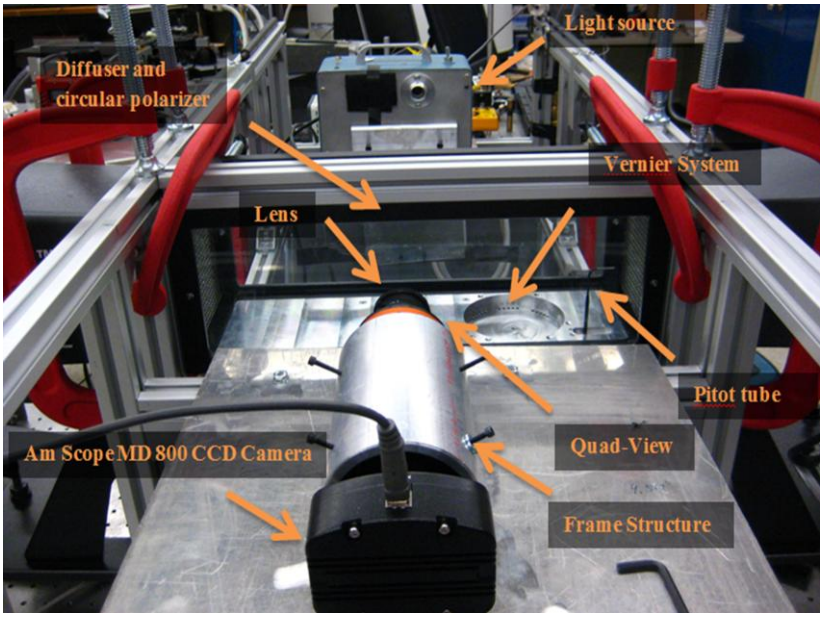

Figure 2.3 Calibration facilities: testing chamber.

Figure 2.2 and 2.3 are images of the testing facilities with detailed description of each component.

2.2 Calibration set up and technique

The calibration tests are conducted in the following way. The sample was first secured inside the test chamber and then tested at a series of speed points. Typical tests consist of speed points at 13, 26, 39, 52, 65 and 80 MPH. In each test, after the sample was secured, an initial birefringence $|sin\delta|$ map was taken and set as the background of the $|sin\delta|$ map. Any new $|sin\delta|$ map collected after this point, therefor would be the result of the real $|sin\delta|$ map subtracting this original $|sin\delta|$ map. As previously mentioned, the non-aligned PDLC films have liquid crystal directors pointing at random directions. By subtracting the initial $|sin\delta|$ map, only the change in $|sin\delta|$ would show up as signal, this improves the signal coherency. After this process is finished the data were collected while the wind tunnel was running at the first speed point. Then the wind tunnel shuts down and another set of data was collected to compare with the initial background to see if any changes occurred. This method tests the repeatability of the PDLC film. Unless otherwise noticed in the description of the test, this process repeats five times before moving on to the next speed point. The overall the experimental inquiry is complete after all five speed points are tested.

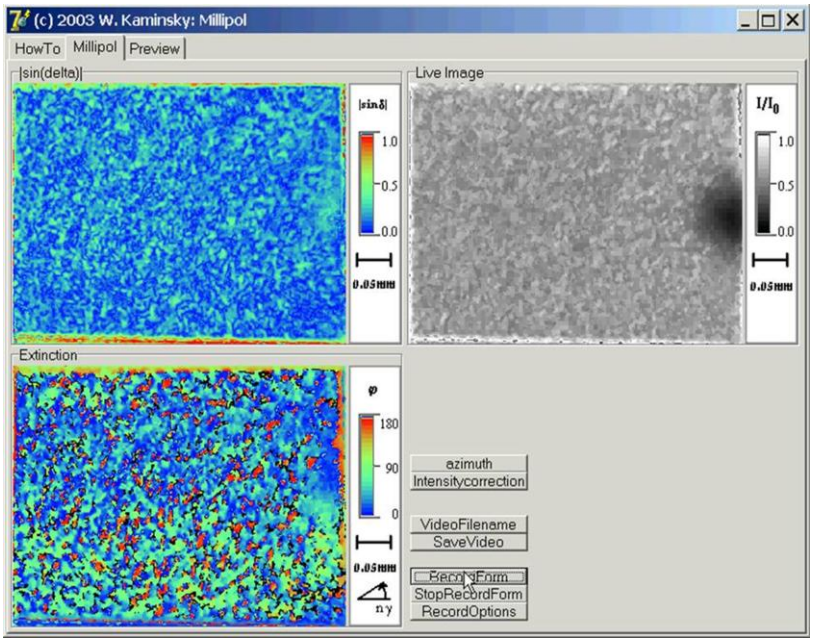

Figure 2.5 MilliView interface. *This displays a sample with no airflow going. As can be seen since there was no alignment, the* $|\boldsymbol{sin\delta}|$ *and* ϕ *are displayed as randomly distributed colors. This image did not subtract the initial birefringence.*

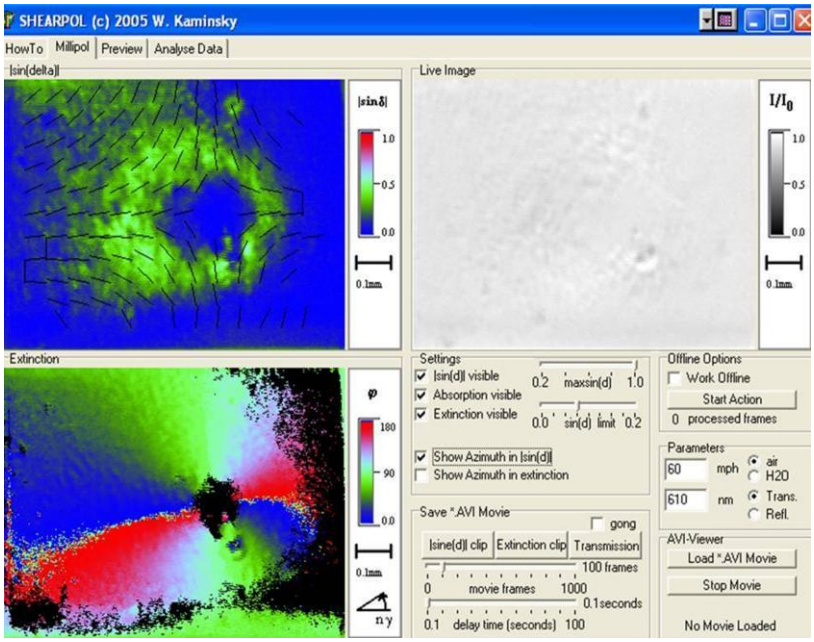

Figure 2.4 MilliView interface (2). *This displays a sample with a jet shooting at the normal direction of the substrate. Both* $|\boldsymbol{sin\delta}|$ *and* ϕ *clearly align according to the shear stress. Though the color scheme may not have enough resolution to distinguish the values, actual values can be read from the map by selecting an area of interest.*

2.3 Data analysis

Data was collected in the "MilliView" system. It displays the $|sin\delta|$ map using a color bar scheme. The $|sin\delta|$ value increases from 0 to 1as the wavelength of the color increase from blue to red. The extinction angle ϕ is displayed in a similar fashion. It increases from 0^o to 180^o as the wavelength of the color increases from blue to red. The "MilliView" interface is illustrated in Fig. 2.4 and Fig. 2.5. Since $|sin\delta|$ and ϕ are displayed at per pixel resolution, data can acquired at same resolution level. Normally an area of interest is selected, instead of analyzing the whole map. "MilliView" displays the average value of the $|sin\delta|$ over the selected area, which was then recorded and plotted for results. Since the tests performed were unidirectional, the extinction angle was not recorded.

The shear stress at each of the speed points was estimated using 1/7 power law derived by Theodore von Kármán as shown in Eq. (15), since the thickness of the micro-slide would trip the flow into turbulence boundary layer even at 13 MPH.

$$C_f = \frac{0.0583}{Re_x^{0.2}}, \tag{15}$$

where C_f is the skin friction coefficient defined in Eq. (16) and Re_x is the Reynolds number based of distance measured from leading edge as defined in Eq. (17).

$$C_f = \frac{\tau_w}{\frac{1}{2}\rho U_\infty^2}, \tag{16}$$

where τ_w is the wall shear stress, ρ is the air density here, and U_∞ is the free stream velocity.

$$Re_x = \frac{\rho x U_\infty}{\mu}, \tag{17}$$

where x is the distance measured from leading edge and μ is the dynamic viscosity of the air here. A plot of the shear stress at 13 MPH is given in Fig. 2.6.

The shear stress correlates to a shear strain according to Eq. 18 as shown below.[37]

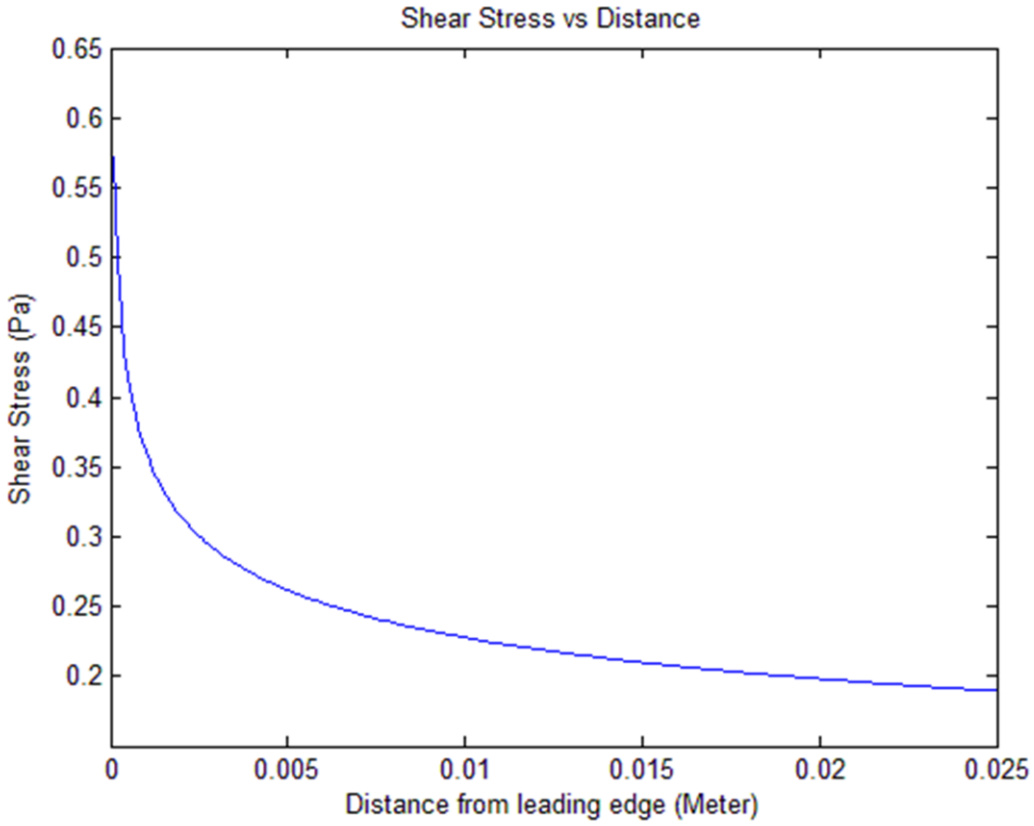

Figure 2.6 Shear stress versus distance at 13 MPH. *The shear stress is plotted over the micro-slide estimated using the 1/7 power law versus distance from leading edge.*

$$\gamma_{xy} = \frac{\tau_w}{G}. \tag{18}$$

The change of the director angle Δθ for an initially aligned PDLC film relates to the shear strain by Eq. 19 as listed below.

$$\Delta\theta = \frac{1}{2}\gamma_{xy}. \tag{19}$$

The signal measured by "MilliView" $|sin\delta|$ can be related to shear stress using Eq. 6,7,18, 19, as expressed below.

$$|sin\delta| = |sin[\frac{\pi}{\lambda}(n_e - n_o)sin^2\left(\frac{1}{2}\frac{\tau_w}{G}\right)L]|. \tag{20}$$

The shear stress can be then related back to velocity using Eq. 15 and 16 as shown below.

$$\tau_w = \frac{0.0583}{2}\rho^{0.8}U^{1.8}\frac{\mu}{X}^{0.5}. \tag{21}$$

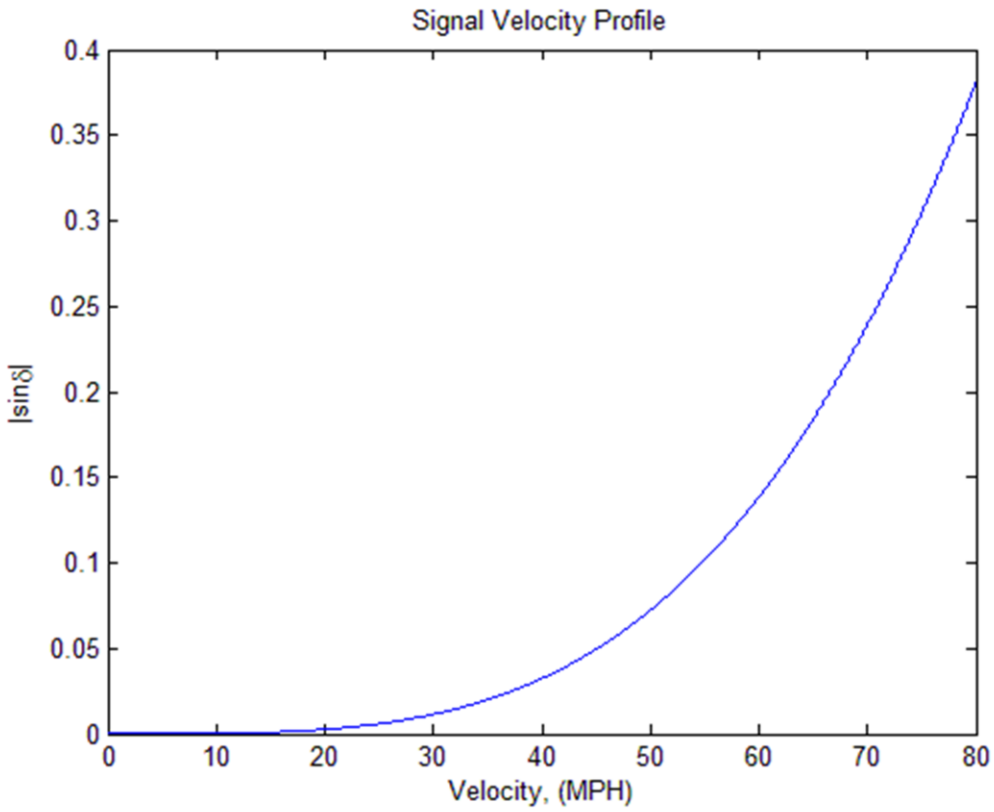

Figure 2.7 Signal Velocity Profile. *A plot of signal versus velocity profile with C_1 equals to10^2 and C_2 equals to 10^{-4}.*

At the same location, neglecting the change in the thickness of the film, the signal $|sin\delta|$ relates to free stream velocity U by Eq. 22,

$$|sin\delta| = |sin[C_1 sin^2(C_2 U^{1.8})]|, \qquad (22)$$

where C_1 and C_2 are defined in the following equations respectively.

$$C_1 = \frac{\pi}{\lambda}(n_e - n_o)L, \qquad (23)$$

$$C_2 = \frac{0.0583}{4G}\rho^{0.8}\frac{\mu}{x}^{0.2}. \qquad (24)$$

For films around 15μm thick, C_1 is on the order of 10^2. However the shear-modulus of the PDLC films is hard to determine, since the structure of PDLC makes it a composite material with liquid-crystal-solid properties. A value of C_2 on the order of $10^{-4}\frac{s}{m}^{1.8}$ is chosen as shown in Fig. 2.7 to demonstrate how the velocity, signal relationship would look like without any particular meaning. This relationship is confirmed in "Results" section through a number of plots.

Chapter 3. Results

3.1 Initial assessment

This experiment was run at the beginning of the project in order to assess the behaviors of polymer-liquid crystal combinations. The polymers that were used in this experiment included Polycarbonate-silicone copolymer (MAX), Poly(bisphenol A carbonate) (PBA) and Poly(butyl methylacrylate) (PBMA). The two liquid crystals that were tested included the chiral nematic NCU-192 (Hallcrest, Inc) and the nematic LC61/E7 (Hallcrest, Inc). A list of all polymers, liquid crystals and solvents used throughout this project is given in Appendix C. The polymer and the liquid crystal combinations were first dissolved in 20 ml vials with dichloromethane at a one-to-one mass ratio and then airbrushed on the glass slide at 20 psi.

These tests were conducted at only four speed points: 20, 40, 60 and 80MPH. In each test the sample was only run at each speed point once. Plots are formatted in the following matter: the red dots indicate the signal at the speed points, the blue dots are the corresponding no wind signal. The average value at each test point based on the three runs is plotted in the bottom right plot of each figure. Results are presented in Fig. 3.1 through Fig. 3.6.

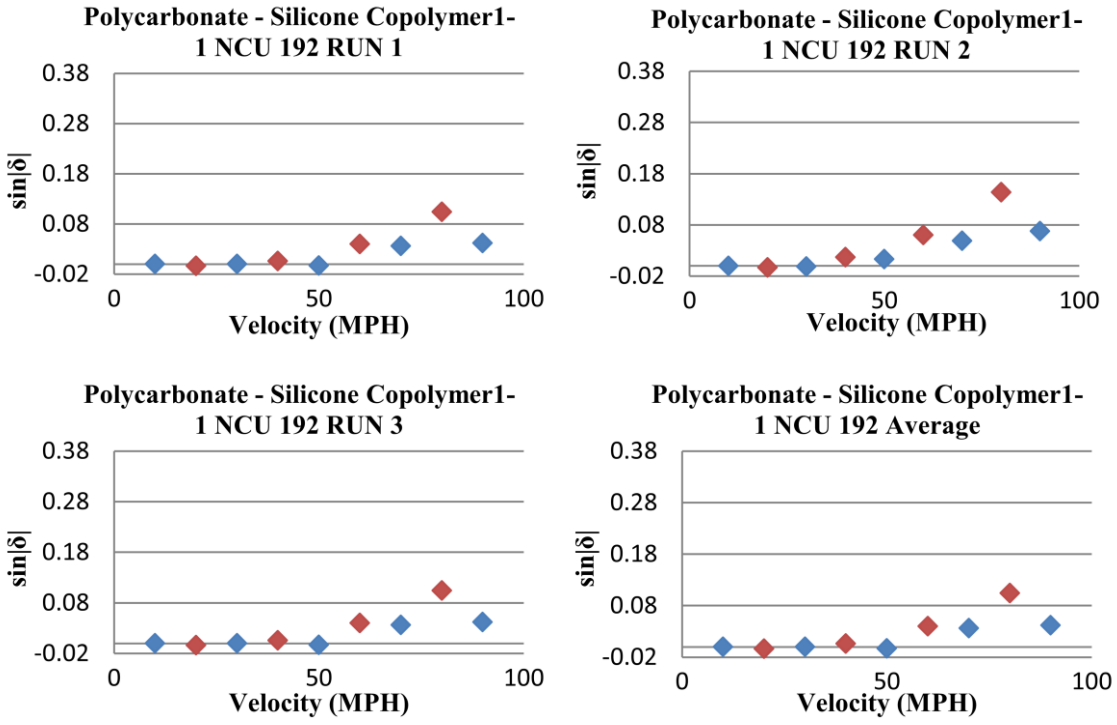

Figure 3.1 Polycarbonate-Silicone Copolymer 1-1 NCU 192.

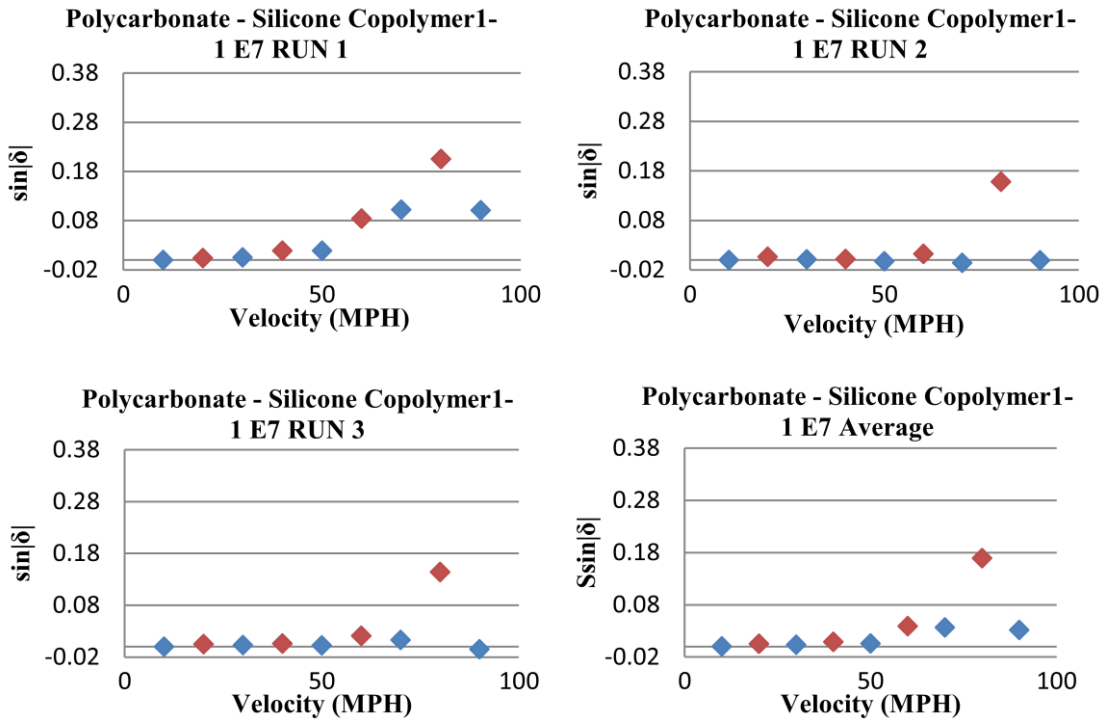

Figure 3.2 Polycarbonate-Silicone Copolymer 1-1 E7.

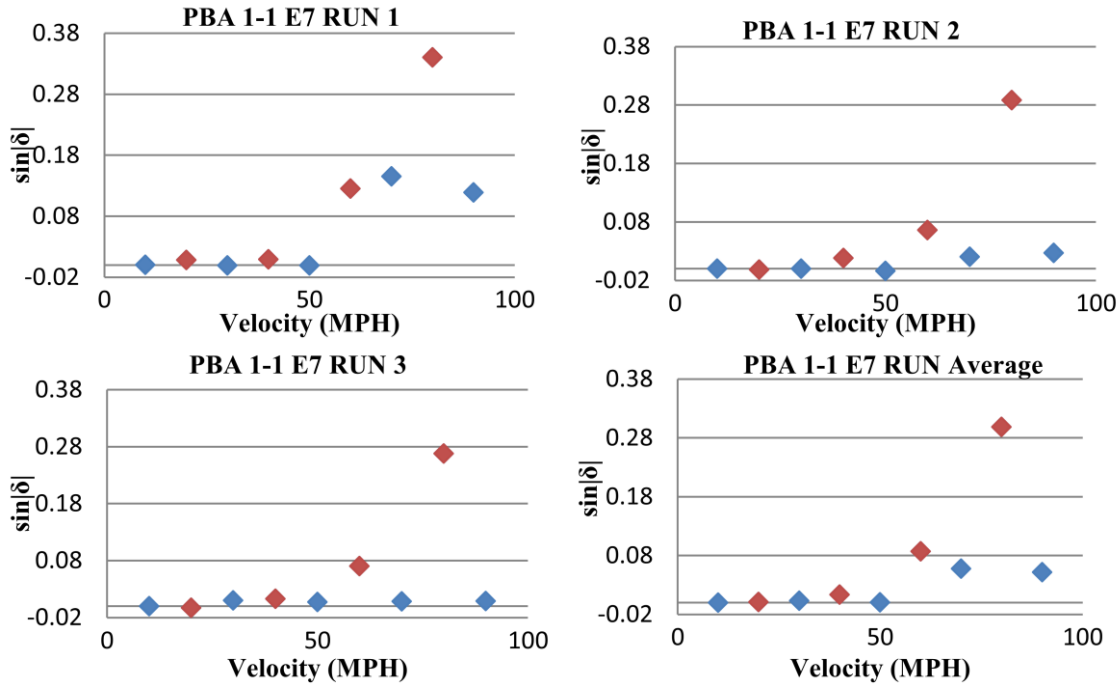

Figure 3.3 PBA 1-1 E7.

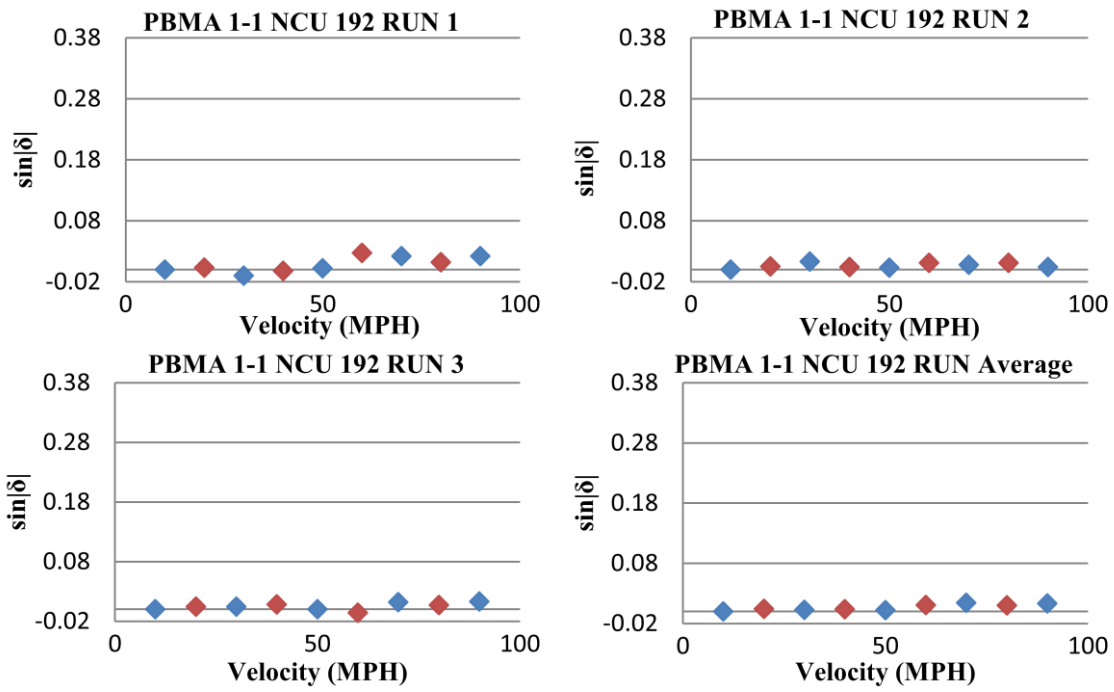

Figure 3.4 PBMA 1-1 NCU 192.

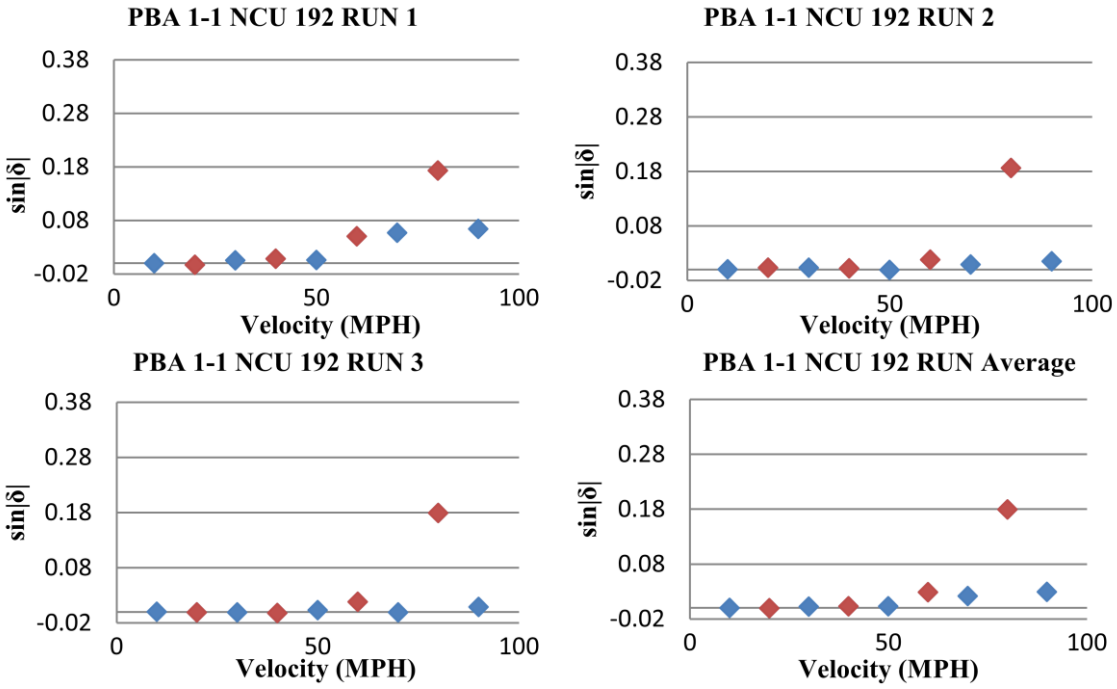

Figure 3.5 PBA 1-1 NCU 192.

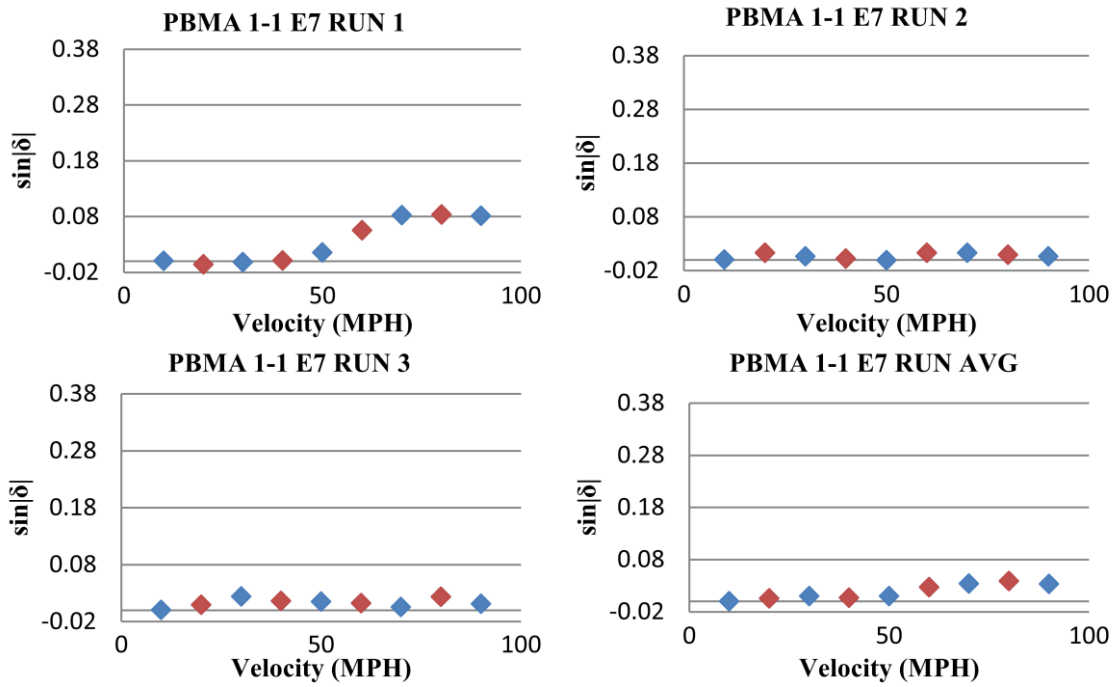

Figure 3.6 PBMA 1-1 E7.

As can been seen in this study, PBA was the most flexible polymer among the three polymers that were tested, since it gave the best signal-to-noise ratio. The E-7 liquid crystal generally had a higher signal strength compared to NCU 192. This initial assessment demonstrated the feasibility and the potential of this project. The PBA and E-7 combination particularly showed a good signal-to-noise ratio and high reversibility. This study also helped us to discover some problems that the system had at the time, such as the reversibility change between the first run and later run. This problem was concluded to have been caused by the vibration movement when the wind tunnel was running. It was later fixed by adding additional C-Clamps to improve the rigidity of the supporting structures.

3.2 Air brushing study

A series of tests were done with all the test samples airbrushed onto the substrates. Airbrushing is one of the few ways that can be tested in a controlled manner. It gives a rather uniform surface finish as compared to other methods. The thickness of the film can be controlled by changing the amount of the solution to be airbrushed onto the substrate.

In this study, the polymer alone was first airbrushed onto the substrate. Then the liquid crystal was sprayed on top of the polymer in two different fashions: revived and non-revived initialed R and N respectively in the figures. In revived fashion, after a specified time from when the polymer was airbrushed, pure solvent was airbrushed onto the polymer substrate. The liquid crystal dissolved in solvent was then airbrushed onto the substrate. In the non-revived fashion, liquid crystal dissolved in the solvent was directly airbrushed onto the polymer substrate at the specified time. The number in the figure title after the initial N or R indicates how many minutes after when the polymer was airbrushed was the solvent or the liquid crystal-solvent mixture airbrushed. Poly(bisphenol A carbonate) (PBA) and Dimethylsiloxane-bisphenol A-polycarbonate block co-polymer (MAX) were the two polymers used in this experiment. The liquid crystal that was used in this experiment is LCR-NCU192. Dichloromethane was used as the common solvent. The tests were done in a typical fashion of having six speed points at 13, 26, 39, 52, 65 and 80MPH and repeating five times at each point. Unless otherwise noted all tests were done in this fashion. The results are shown in Fig. 3.7 to Fig. 3.10.

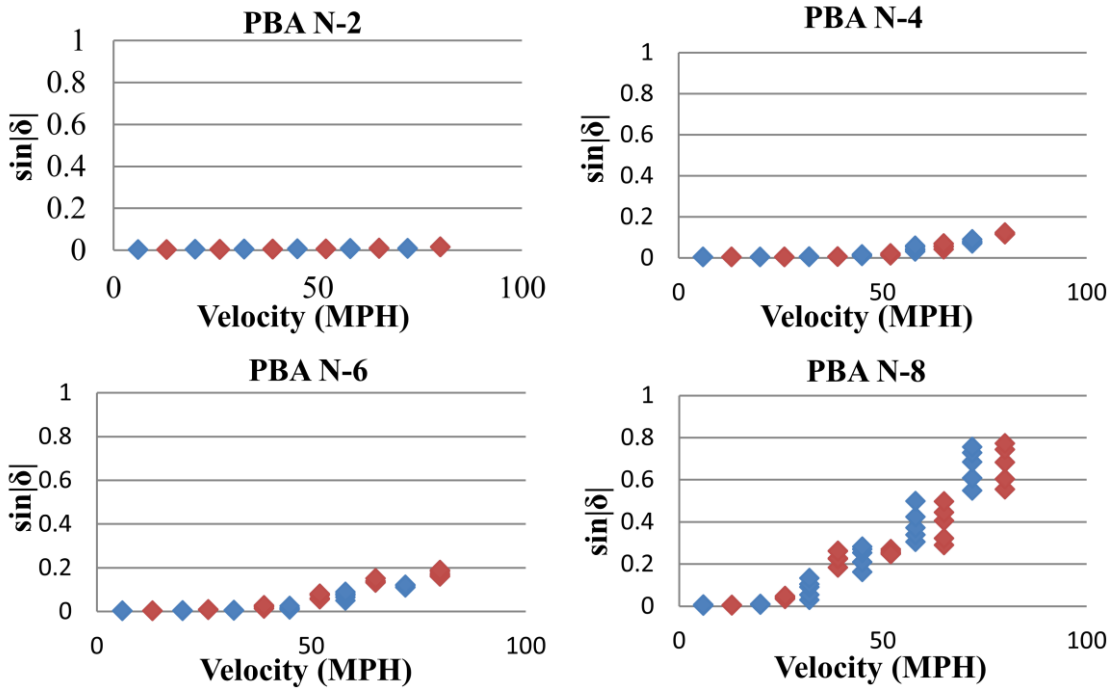

Figure 3.7 PBA NCU-192 Non-revived

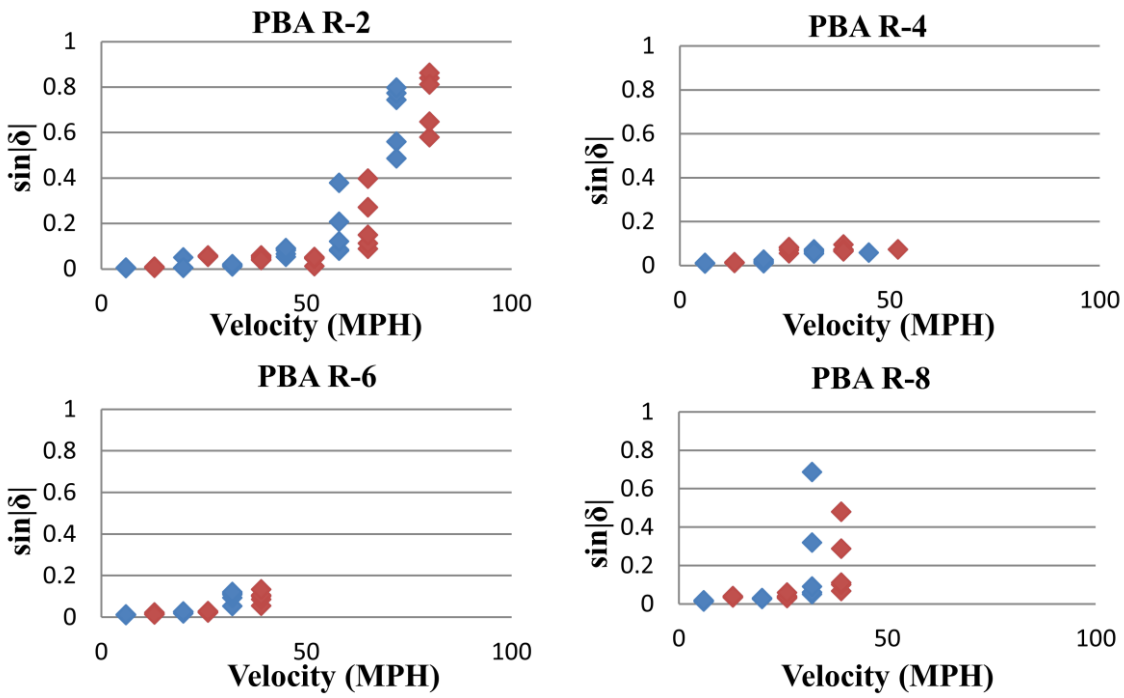

Figure 3.8 PBA NCU-192 Revived

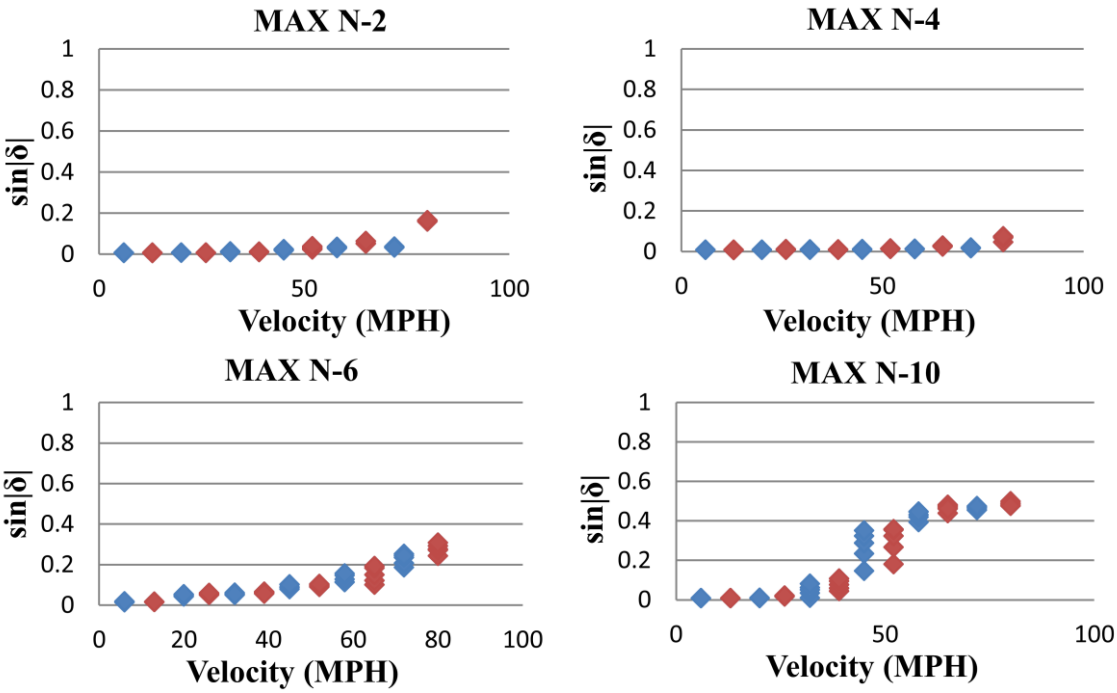

Figure 3.9 MAX NCU-192 Non-revived

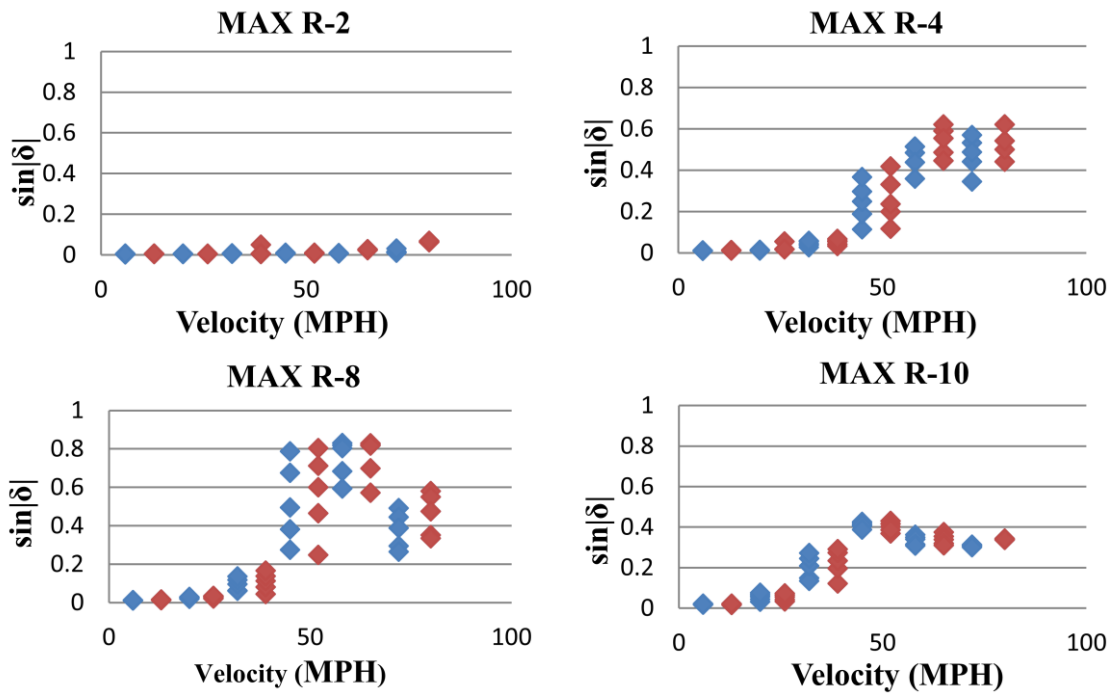

Figure 3.10 MAX NCU-192 Revived

This test demonstrated the classic gain-bandwidth tradeoff phenomenon of sensing technology. The non-revived cases clearly provided a stronger bond between the liquid crystal layer and the polymer layer. This was demonstrated by the lower signal strength in the non-revived cases. At the same time, it also showed better reversibility. Thus it has higher temporal bandwidth. Another trend observed in this test is that as the waiting time increased the bonding strength between the two layers became weaker. The contradicting results shown in MAX R-8 and MAX R-10 in Fig. 3.10 are because the liquid crystal layer was blown off the polymer layer at high wind speed. The unfinished test in Fig 3.8 is due to the same reason. The data collected after the liquid crystal layer was blown off no longer possess any meaning. The difference between the two polymers cannot be clearly concluded in this test. The limited data does not show a conclusive trend.

3.3 Poly(methyl methacrylate) study

In this study a combination of Poly(methyl methacrylate) (PMMA) and the nematic liquid crystal E-7 was tested. This new polymer was suggested by Dr. John, West. at Kent State University. An attempt of using rubbed Polyvinyl alcohol (PVA) to align the liquid crystal droplet within the PDLC film was also studied. Two PDLC samples were compared side by side here. Both solutions were made of PMMA and E-7 dissolved in dichloromethane at a one-to-one mass ratio

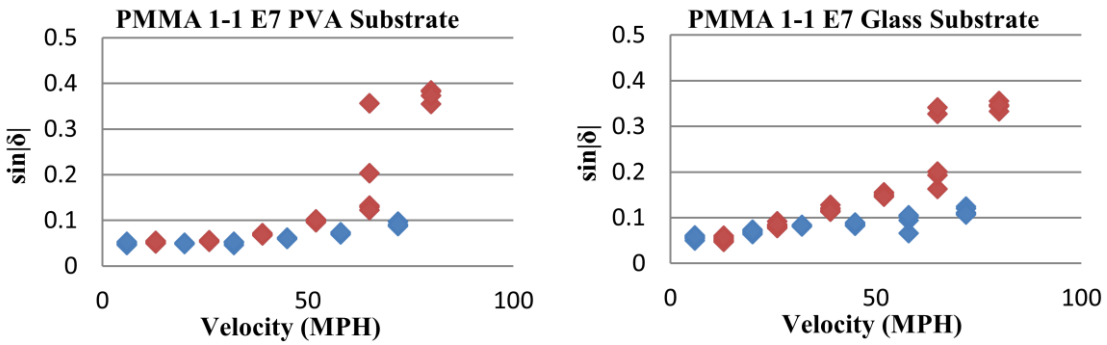

Figure 3.11 PMMA 1-1 E7.

by weight. The PVA was dissolved in hot water and then deposited on top of one of the micro-slides. The PVA film was a clear and uniform film after it was completely cured. It was then mechanically rubbed with a velvet cloth in a unidirectional fashion. This is a well-known technique to align nematic liquid crystals. The theory is that the microgrooves formed on top of the polymer film due to this mechanical rubbing will align the liquid crystal directors along the direction of the grooves. Based on this theory, the assumption in this study was that the liquid crystal droplets would behave similarly to liquid crystal in these microgrooves. After the rubbed PVA substrate was prepared, the solution of PMMA and E-7 combination was directly deposited on top of this substrate as well as a regular glass substrate. The results of this test are shown in Fig. 3.11.

Both of the samples presented better characteristics including high signal-to-noise ratio and high reversibility over the previously studied samples. However the attempt of using a rubbed PVA substrate to align the PDLC film failed. Both films presented strong scattering effects and a rough surface. They both formed goose-bump like structures on the surface; each bump had very strong scattering effect. This suggested the liquid crystal directors were not aligned across different droplets. This hypothesis was confirmed when the birefringence of the samples were visualized in the "MilliView" software. The inconsistent result at 65MPH was theorized to be due to how the sensor responds with respect to time. It has been observed that at this wind speed, the sensor had a fast initial response to the shear stress, however, with relatively lower signal strength. As the shear stress was sustained, the signal increased gradually. After this there was a sudden jump in signal strength. Then the signal remained at that value. Thus signal level

would vary according to what time relative to the experiment the data was collected. This phenomenon also presented at 80MPH, however the sudden jump happened almost immediately as the wind tunnel turned on. Thus, the results at 80MPH show more consistency. The gradual increase was theorized as being part of the strain stress relationship of the PDLC films. The sudden jump was theorized as being due to the sample slightly tipped over at high wind speed, due to a failure of structure support. This was improved by adding more structure supports.

3.4 Application methods study with PMMA

Continuing the successful results found with the PMMA and E-7 combination, a series of samples using the same combination were tested in this study. However this test was focused on the application methods such as airbrushing, direct depositing and spin-coating. In the airbrushing method, toluene was added to the solution to control the curing rate. With pure dichloromethane the solution tends to cure before it even reaches the substrate. This resulted in the films to have an undesirable surface finish. The added toluene helped the solution to cure at a slower rate. In spin coating, the solution was first poured on top of a glass micro-slide. It was then put in a Clay Adams Readacrit Centrifuge. A TDGC - 3KM metered variable autotransformer was connected to the centrifuge to control the spin rate. An airbrushed PMMA and NCU 192 sample was also tested in this study. Results are presented in Fig. 3.12.

The spin coated sample gave a clear film with a smooth and uniform surface. The clearness in the film indicated the droplet size of the liquid crystal was smaller than the wavelength of the visible light. The only other explanation would be that the spinning motion aligned the directors of liquid crystal droplets. This was highly unlikely to happen and was confirmed by the birefringence-map taken by the "MilliView". The spin coated sample, therefore, had almost no signal over the majority of the film are with the exception happened on the edge of the film. Data was taken over a small area on the edge of the film. In the airbrushed sample, the sample presented a smooth and uniform surface with an opaque film. This is similar in both of the airbrushed samples. The NCU 192 combination showed a colorful opaque film compared to the white opaque film of the E7 combination. The difference is due to the nature of the chiral nematic liquid crystal.

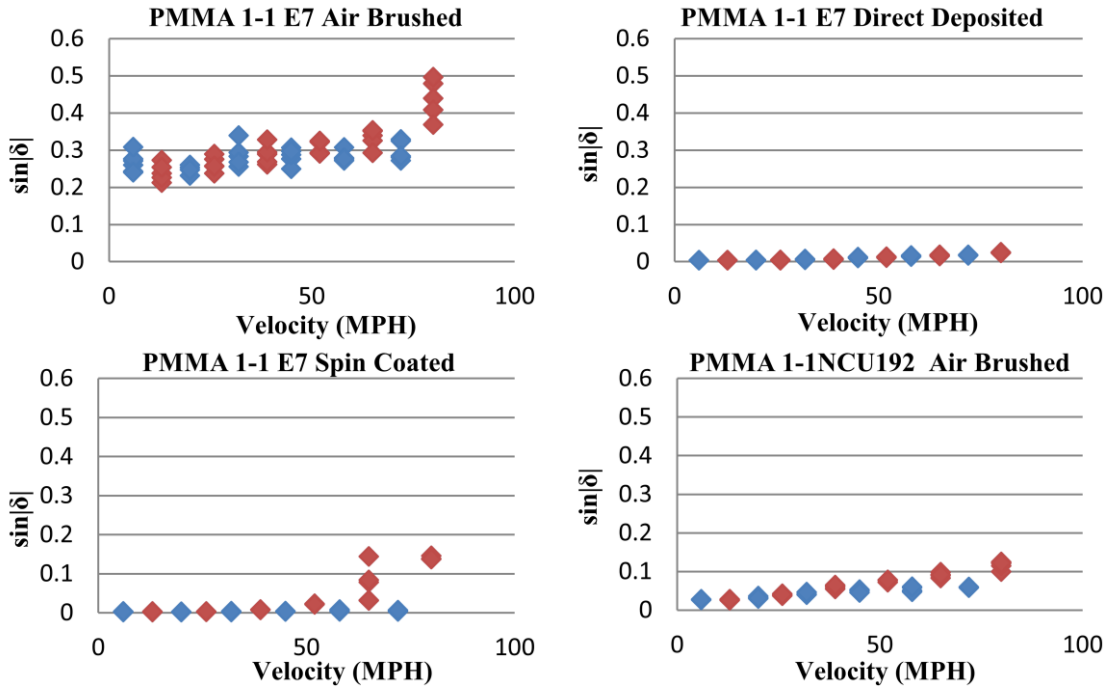

Figure 3.12 Application methods study.

The directly deposited sample used a heated solution of PMMA and E7. This gave the sample a more uniform and smooth surface compared to the previous study. It also retained its strong scattering effect. The overall results of this study are unsatisfying compared to the previously study of the PMMA and E7 combination. This study showed the importance of the application methods. Both the thickness of the film and the curing rate of the film significantly affected the performance of the sensor.

3.5 Direct deposition study

In the previous two studies, the directly deposit method showed more promising results. Despite its disadvantages such as a non-uniform surface and thickness, it was used again in this study. A new polymer, polystyrene was introduced in this study. This is the polymer used by Parmer [33] *et al*. in their study of PDLC film. Polycarbonate and PMMA were also used in this study. Both the NCU 192 and E7 were tested with all polymers. Results are presented in Fig. 3.13.

As can been seen, the E7 clearly presented better characteristics in this study, compared to the more viscous NCU 192. It had a much better signal-to-noise ratio. The PMMA and the E7 combination showed a poor performance compared to the two previous studies. This again showed the importance of improving uniformity in manufacturing techniques. The polystyrene and the E7 combination presented great qualities in this study. It had coherent signal at as early as 39MPH and showed high signal strength and reversibility.

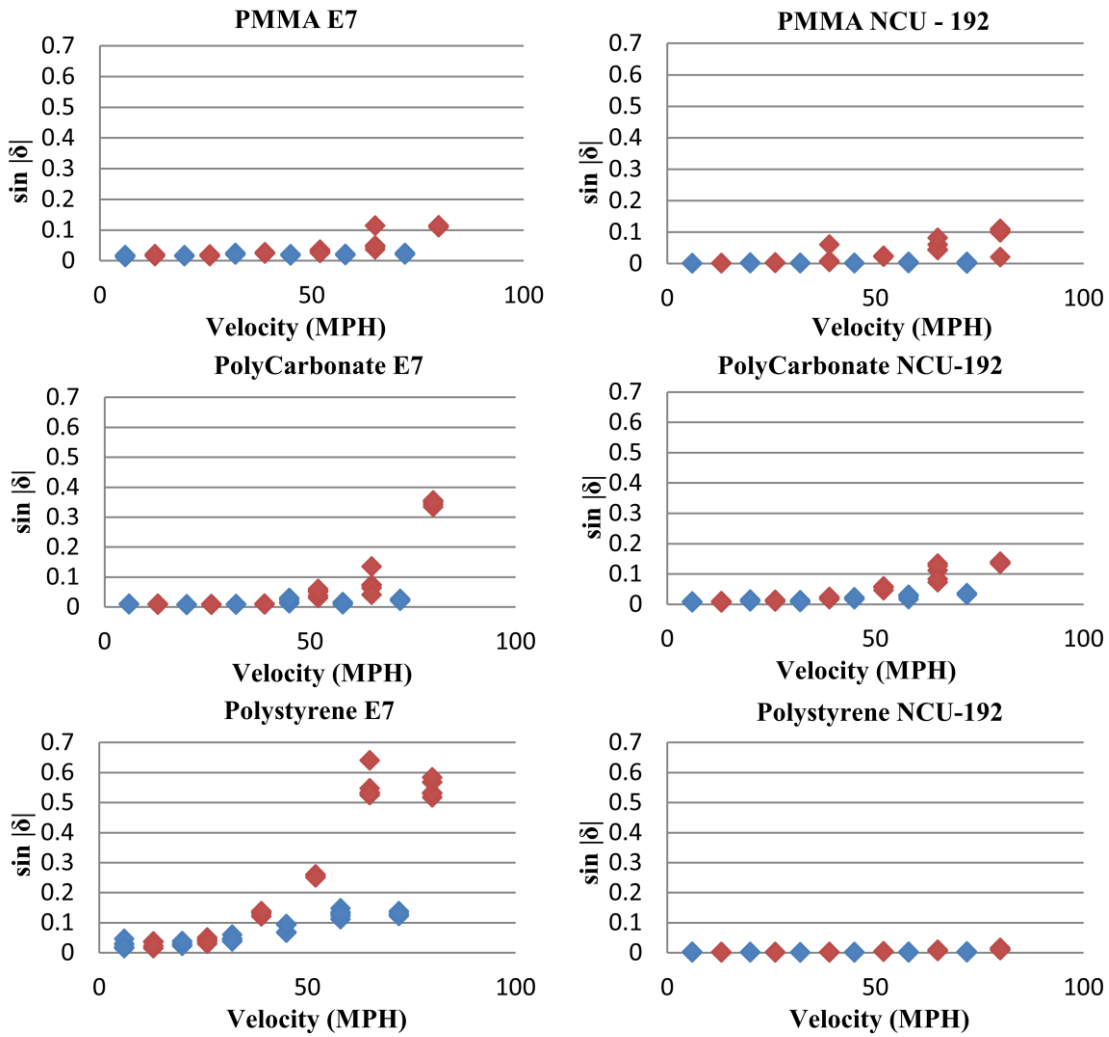

Figure 3.13 Direct deposit study. *Note: Poly(bisphenol A carbonate) is denoted Polycarbonate in this figure.*

3.6 E7 study

As was learned from the previous study, the E7 liquid crystal clearly presented a better signal-to-noise ratio. Thus, in this study only E7 was tested with various polymers using a direct deposition method. Two new polymers were introduced here: Fluorinated Acrylic (FIB) and Polysilicone. Compared to other polymers, FIB needs a special solvent, trifluorotoluene to dissolve. The Polysilicone used in this test on the other hand would only cure after hardener was mixed in. Two Polysilicone E7 samples were made. In sample A, the liquid crystal was directly mixed with Polysilicone and hardener, before being deposited on top of the glass micro-slide substrate. In sample B, the mixture of E7, Polysilicone and hardener was dissolved in toluene, before being applied on the substrate. Results are given in Fig. 3.14.

The Dimethylsiloxane-bisphenol A-polycarbonate block co-polymer (MAX) and E7 combination showed the best results obtained thus far. Though the signal strength is not as high as a few other combinations such as FIB and E7 as well as PMMA and E7, it showed a coherent signal at as early as 13MPH. It also had a linear response to the velocity, is highly consistent over each test points, and is highly reversible. The FIB and E7 combination showed similar desirable characteristics.

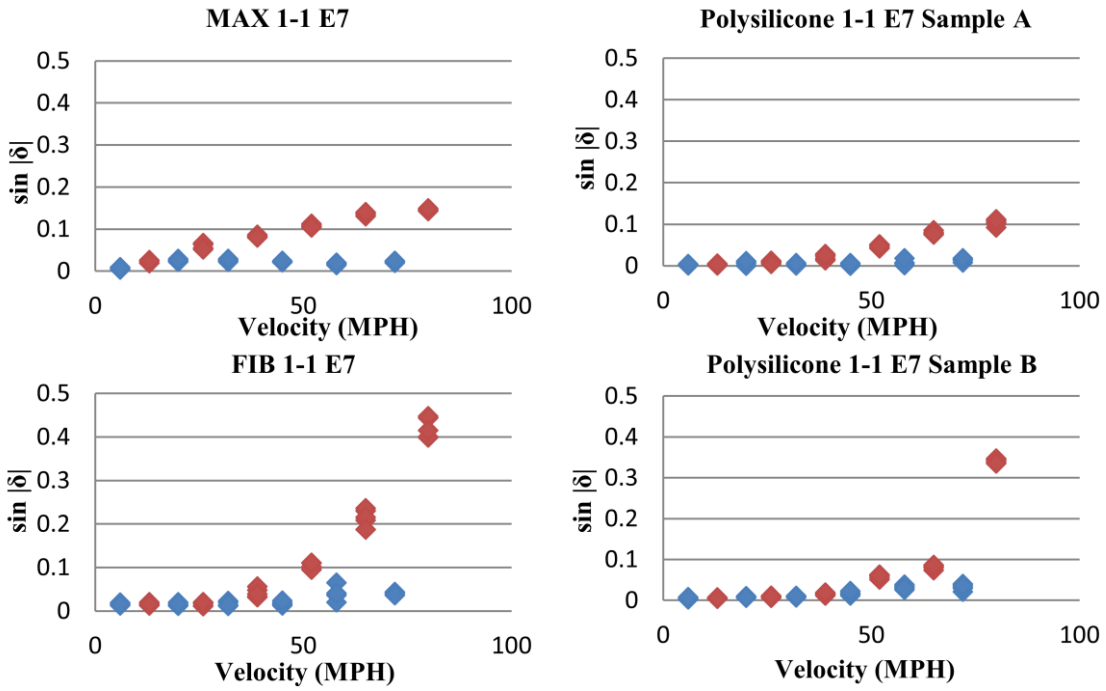

Figure 3.14 E7 Study.

3.7 Reproducibility test

In this test the reproducibility of the sensor was studied. The previously used MAX and E7 combination sample was tested in this study after two weeks of room storage. This test was done in a different manner. The results are shown in Figure 3.15. It was plotted in the following fashion, from left to right, the sample was tested at 0, 13, 0, 26, 0, 39, 0, 52, 0, 65, 0, 80, 0, 65, 0, 52, 0, 39, 0, 26, 0, 13, 0MPH. Each speed point was only tested once. The blue dots are at 0MPH and the red dots are at the speed points. The overall result of this study was satisfying. Except of the results at 65MPH, it was highly consistent and highly reversible.

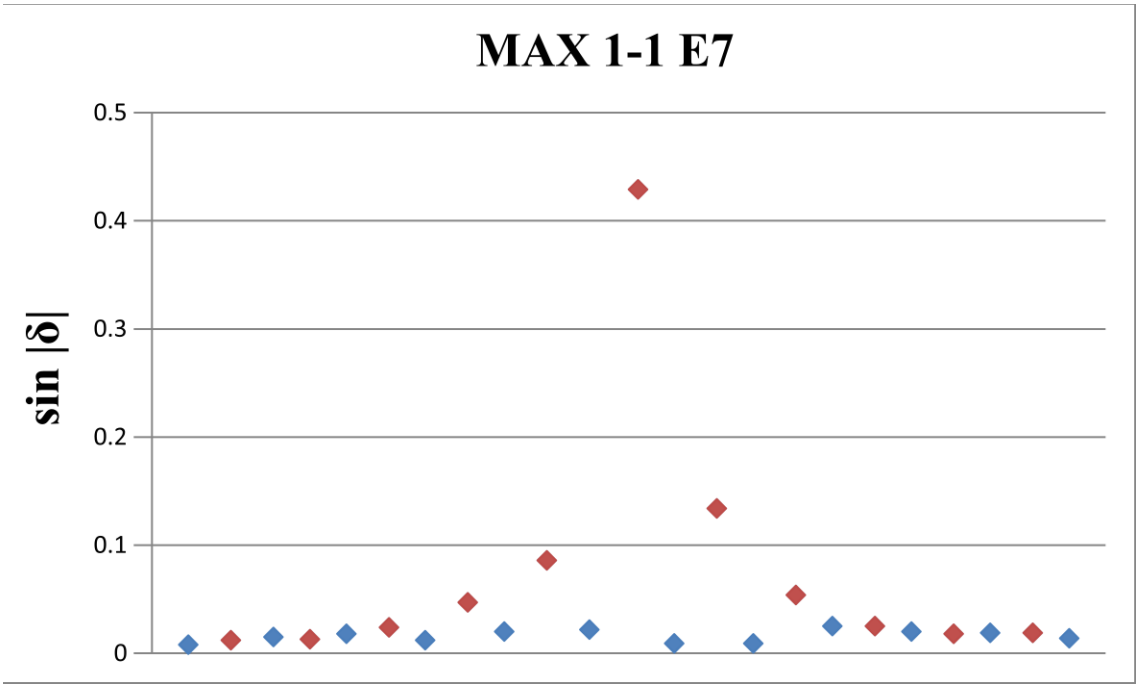

Figure 3.15 Reproducibility test.

Chapter 4. Future works

For PDLC to become a practical solution to provide 2-D shear stress map, there remains a significant amount of works needed to be done on this project.

4.1 Uniformity improvement

The uniformity of the PDLC samples must be improved. Fabrication techniques must be improved in such a way that the film can be reproduced using the same technique. Details such as surface smoothness, droplet size, and film thickness, especially the latter two cases, need to be controlled through proper fabrication techniques. This would provide the capability of analyzing how these details affect the performance of the PDLC films thoroughly.

4.2 Response time study

As in all sensing technologies, the temporal resolution of the sensor determines the capability of it. Therefore it is very important to characterize the temporal resolution of the PDLC films. The Am Scope MD 800 E color CCD camera can only record videos at 30 fps. Thus the temporal bandwidth of the PDLC films can only be studied at this resolution at the best. Equipment has higher temporal resolution is required to determine the temporal characters of the PDLC films properly. A simple set up with a photodiode and high speed data acquisition (DAQ) card can achieve this goal.

4.3 Liquid crystal alignment

As previously mentioned, the randomly aligned liquid crystal droplets cause a strong scattering effect in the PDLC film. This limits the thickness of the PDLC film that can be used. If the films are too thick this scattering effect would not be able to provide enough light passing through the film for the birefringence to be studied. Another importance of this technique is that the aligned liquid crystal droplets would theoretically improve the signal-to-noise ratio of the PDLC film. The alignment would allow all the droplets inside the PDLC film to respond to the shear stress uniformly, therefore, improve the signal coherency. These improvements are especially important if a reflective method to be developed. One of the feasible alignment techniques at current is

to impose an electric field while the PDLC is curing. The liquid crystals used in PDLC, therefore, must be ferroelectric for this to happen. The nematic liquid crystal E-7 that was used in this study is an example of a ferroelectric liquid crystal.

4.4 Reflective method

The development of a reflective method is a key step for the PDLC sensors to become practical. The current backlight technique would require the substrate to be transparent. This sets a stringent limit to what kind of surface the sensors can be tested on. Since the majority of the wind tunnel models are not transparent, a reflective lighting method becomes the clear solution to this problem. The aforementioned light scattering effect imposes a challenge on this development. In a reflective lighting method, light needs to pass through the film at least twice to be detected. This increases the scattering effect dramatically. Thus, liquid crystal alignment is critical to this development.

4.5 Curved surface measurement

Measuring on curved surfaces presents challenges such as curvature-induced birefringence, making calibration difficult. Without a proper aligning technique, the curvature of the substrate can induce a strong birefringence. Though initial birefringence subtraction can help this problem, it also limits the "MilliView" capability such as direction detection. Another problem arises when using the reflective lighting method, the elliptically polarized light reflecting off the curved substrate may induce changes in the extinction angle. This poses great challenges for calibration, perhaps even limiting the technique to in-situ calibrations on different surfaces.

4.6 Calibration against analytical solution

The current shear stress model used in this study is based on the 1/7 power law. This is an empirical model that is based on a lot of assumptions. Calibration against an analytical solution would gain a better understanding of how the PDLC behaves. Proper setups are needed for this to be achieved. On a flat substrate, this can be accomplished by a simple model such as channel flow. On the curved surface, this can be done through using a 2-D NACA 0015 airfoil. In both cases analytical solutions at low Reynolds number are well studied and can be used to calibrate the PDLC sensor.

4.7 Adding pressure sensitive paint (PSP)

As mentioned in the introduction, shear stress and pressure are the two sources of all fluid mechanical forces. Unlike shear stress measurement, 2-D pressure measurement has long been achieved accurately with high spatial and temporal resolution through the use of pressure sensitive paint (PSP) techniques. If the PDLC sensor can have PSP added into the film then, this sensory system would be able to provide 2-D shear stress as well as pressure measurement. This will significantly improve the capacity of this technology.

Chapter 5. Conclusion

This paper demonstrated the feasibility and the potential of using the PDLC film as a shear stress sensor. It is one of the most promising technologies in the field to provide 2-D shear stress measurement. There are a few samples studied in this paper have shown high signal-to-noise ratio and high repeatability. Its non-intrusive nature, high spatial resolution, and high reusability make it a practical solution for use in commercial wind tunnel setups. Though only measuring in two dimensions it still can help gain insight into 3-D phenomena such as the turbulence boundary layer, making the technology valuable in the academic field as well. Another academic and commercial purpose for this sensor is to confirm computational fluids dynamics (CFD) results. Direct numerical simulation (DNS) cannot yet be done on a large scale such as a transport jet. Results from CFD still need calibration and PDLC films provide the capability for this purpose. Drag reduction studies can also be benefited from the PDLC films. It might even be used as a source of a feedback signal for an active drag reduction scheme.

Chapter 6. References

[1] MadouM. Fundamentals of microfabrication.New York: CRC Press, 1997.

[2] Schmidt MA, Howe RT, Senturia SD, Haritonidis JH. Design and calibration of a microfabricatedfloatingelementshear-stress sensor. Trans Electron Dev1988;ED-35:750–7.

[3]Goldberg HD, Breuer KS, Schmidt MA. A silicon waferbondingtechnology for microfabricated shear-stress sensors with backside contacts. In: Technical Digest, Solid-State Sensor and Actuator Workshop, 1994.p. 111–5.

[4] Ng K, Shajii J, Schmidt MA. A liquid shear-stress sensor using wafer-bonding technology. J MicroelectricalmechanicalSyst 1992;1(2):89–94.

[5] Naughoton J and Sheplak M 2002 Modern developments in shear-stress measurement. Prog.Aerosp.Sci 38 515-570

[6] Padmanabhan A. Silicon micromachined sensors and sensor arrays for shear-stress measurements in aerodynamic flows. PhD thesis, Mechanical Engineering Department, Massachusetts Institute of Technology,Cambridge, MA, USA 1997.

[7] Pan T, Hyman D, Mehregany M, Reshotko E, GarverickS. Microfabricated shear-stress sensors, part 1: design and fabrication. AIAA J 1999;37(1):66–72.

[8] Hyman D, Pan T, ReshotkoE, Mehregany M. Microfabricated shear-stress sensors, part 2: testing and calibration. AIAA J 1999;37(1):73–8.

[9] Padmanabhan A, Goldberg HD, Schmidt MA, Breuer KS. A wafer-bonded floating-element shear-stress microsensor with optical position sensing by photodiodes. J MicroelectricalmechanicalSyst 1996;5(4):307–15.

[10] Padmanabhan A, Sheplak M, Breuer KS, Schmidt MA.Micromachined sensors for static and dynamic shear-stress measurements in aerodynamic flows. In: Technical Digest, Transducers '97, Chicago, IL, 1997. p. 137–40.

[11] Padmanabhan A, Schmidt MA, Breuer KS. A silicon micromachined sensor for shear-stress measurements in aerodynamic flows.AIAA Paper 96-0422, 1996.

[12] Sheplak M, Padmanabhan A, Schmidt MA, Breuer KS. Dynamic calibration of a shear-stress sensor using stokes layer excitation. AIAA J 2001;39(5):819–23.

[13] Winter KG. An outline of the techniques available for the measurement of skin-friction in turbulent boundary layers.ProgAerospSci 1977;18:1–57.

[14] Elvery D, Brehorst K. Directional sensitivity of wall mounted hot-film gauges. Meas Sci. Technol. 7 1996.p 1410-1417.

[15] Haselbach F and Nitsche W. Calibration of single-surface hot films and in-line hot films array in laminar or turbulent flows. Meas Sci. Technol. 7 1996.p 1428-1438.

[16] Chandrasekaran V, Cain A, Nishida T and Sheplak M. Dynamic calibration technique for thermal shear stress sensors with variable mean flow. AIAA 2000-0508.

[17] Naqwi AA, Reynolds WC. Dual cylindrical wave laser-Doppler method for measurement of skin-friction in fluid flow.Tech. Rep. Report No. TF-28, Stanford University,1987.

[18] Fourguette D, Modarress D, Taugwalder F, Wilson D, Koochesfahani M, Gharib M. Miniature and MOEMS flow sensors. AIAA Paper 2001-2982, 2001.

[19] Große S and Schröder W. Mean wall-shear stress measurements using the micro-pillar shear-stress sensor MPS^3. Meas. Sci. Technol. 19 2008 015403

[20] Große S and Schröder W. Two-Dimensional Visualization of Turbulent Wall Shear Stress Using Micropillars. AIAA Journal Val. 47, No. 2, February 2009
[21] Haritonidis JH. The measurement of wall shear-stress. In: Gad-el-Hak M, editor. Advances in fluid mechanics.Berlin: Springer, 1989. p. 229–61.
[22] Squire LC. The motion of a thin oil sheet under the steady boundary layer on a body. In: Maltby RL, editor. Flow visualization in wind tunnels using indicators. AGARDograph
70, 1962. p. 7–23.
[23] Tanner LH, Blows LG. A study of the motion of oil films on surfaces in air flow, with application to the measurement of skin-friction. J Phys E 1976;9(3): 194–202.
[24] Monson DJ, Mateer GG, Menter FR. Boundary-layer transition and global skin-friction measurement with an oil-fringe imaging technique. SAE Paper No. 932550,1993.
[25] Mateer GG, Monson DJ, Menter FR. Skin-friction measurements and calculations on a lifting airfoil. AIAA J 1996;34(2):231–6.
[26] Tanner LH, Kulkarni VG. Viscosity balance method of skin-friction measurement: further developments including applications to three-dimensional flow. J PhysE 1976;9:1114–21.
[27] Reda DC. Liquid crystals indicate directions of surface shear-stresses. NASA Tech Briefs 1996;20(5):89.
[28] Reda DC, Wilder MC, Farina DJ, Zilliac G. New methodology for the measurement of surface shear-stress vector distributions. AIAA J 1997;35(4):608–14.
[29] Reda DC, Wilder MC.Shear-Sensitive Liquid Crystal Coating Method Applied Through Transparent Test Surfaces. AIAA J 2001;39 p 195-197
[30] Fujisawa N, Oguma Y and Nakano T. Measurement of wall-shear-stress distribution on NACA 0018 airfoil by liquid-crystal coating and near-wall particle image velocimetry (PIV). Meas. Sci. Technol 20.2009
[31] Buttsworth DR, Elston SJ, Jones TV. Directional sensitivity of skin-friction measurements using nematic liquid crystal. Meas Sci Technol 1998;9(11):1856–65.
[32] Reda, D.C., Murature, J.J., and Heineck, J.T., "Time and flow-direction response of shear-stress-sensitive liquid crystal," AIAA Journal, Vol. 39, Issue 4, APR 1994, pp. 195-197.
[33] Parmar, D.S. and Singh, J.J., "Partially exposed polymer dispersed liquid crystals for boundary layer investigations," Applied Physics Letters, 61, 2039(1992).
[34] Glazer, A.M., Kaminsky, W., and Zysset, P.K., "An automatic optical imaging system for birefringent media," Proceedings of the Royal Society of London Series A-Mathematical Physical and Engineering Sciences, Vol. 452, Issue 1955, Dec 8 1996, pp. 2751-2765.
[35] Kaminsky, W., Gunn, E., Sours, R., and Kahr, B., "Simultaneous false-colour imaging of birefringence, extinction and transmittance at camera speed," Journal of Microscopy-Oxford, Vol. 228, Issue, NOV 2007, pp. 153-164.
[36] Spiese, E.M., Kaminsky, W., and Zysset, P.K., "A quantitative collagen fibers orientation assessment using birefringence measurements: Calibration and application to human osteons," Journal of Structural Biology, Vol. 176, Issue 3, DEC 2011, pp. 302-306
[37] Richard G. Budynas "Advanced Strength and Applied Stress Analysis" Second Edition WCB/McGraw-Hill, 1999, ISBN007008985X, 9780070089853

Appendix A

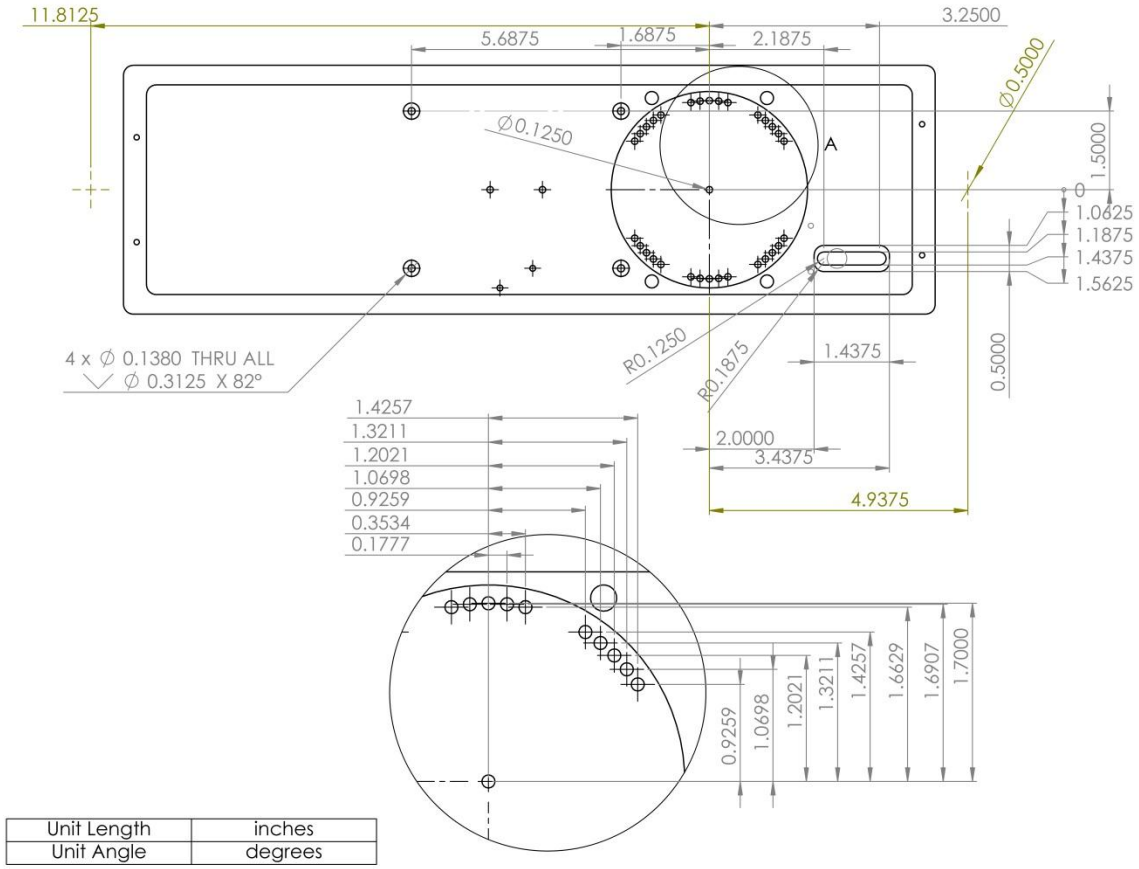

Unit Length	inches
Unit Angle	degrees

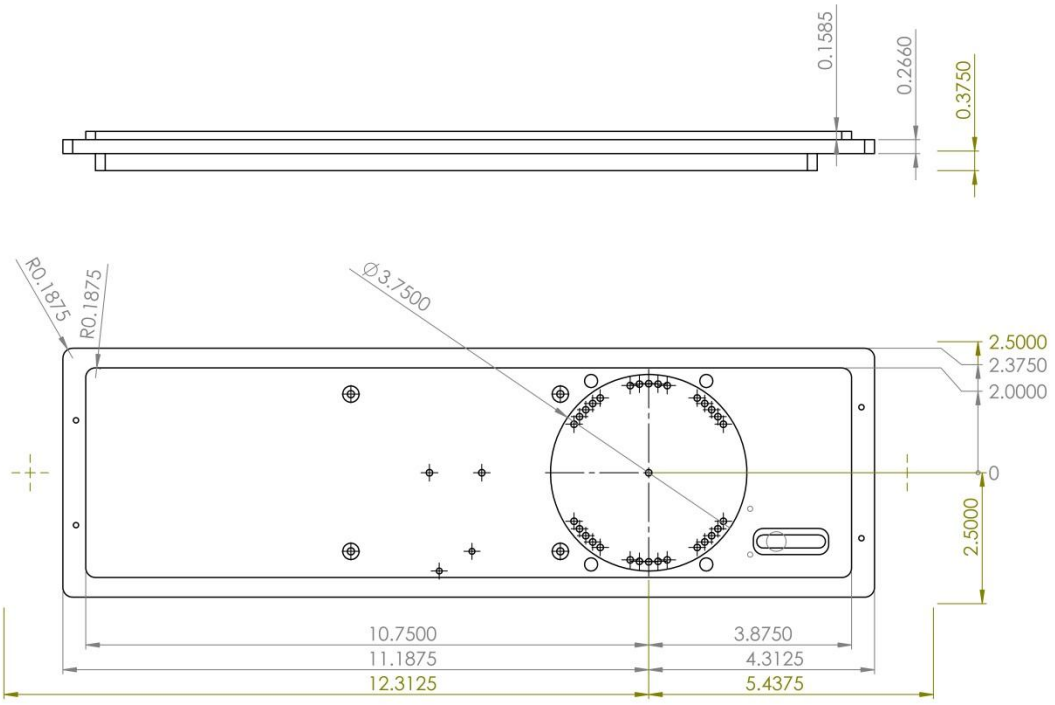
0.1585
0.2660
0.3750
R0.1875
R0.1875
∅3.7500
2.5000
2.3750
2.0000
0
2.5000
10.7500
11.1875
12.3125
3.8750
4.3125
5.4375

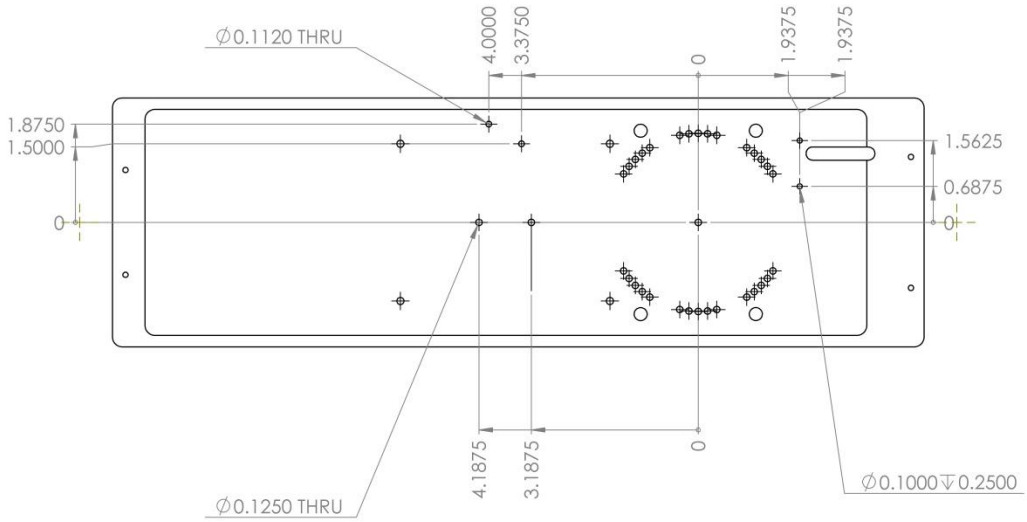
∅0.1120 THRU
4.0000
3.3750
0
1.9375
1.9375
1.8750
1.5000
1.5625
0.6875
0
0
4.1875
3.1875
0
∅0.1250 THRU
∅0.1000↧0.2500

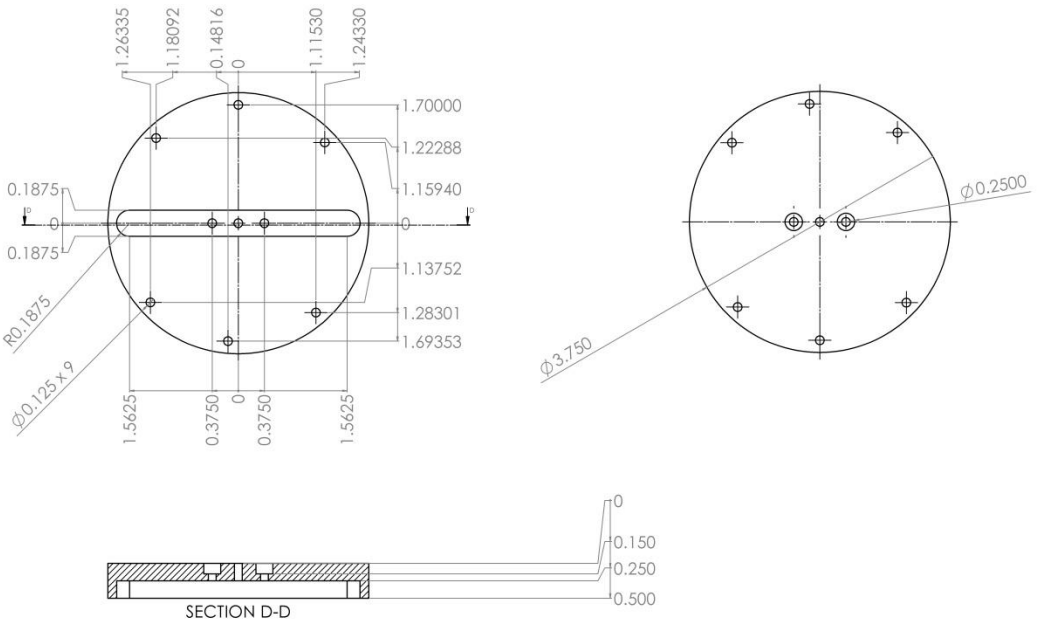
1.26335
1.18092
0.14816
0
1.11530
1.24330
1.70000
1.22288
1.15940
0.1875
0
0.1875
1.13752
R0.1875
1.28301
1.69353
Ø0.125 x 9
1.5625
0.3750
0
0.3750
1.5625
Ø0.2500
Ø3.750
0
0.150
0.250
0.500
SECTION D-D

Appendix B

computar

H2Z0414C-MP

2X 4-8mm F1.4
for 1/2 type Megapixel cameras, Vari-focal Manual Iris
C-Mount

Model No.		H2Z0414C-MP		Effective	Front	φ22.2mm	
Focal Length		4mm - 8mm		Lens Aperture	Rear	φ10.7mm	
Max. Aperture Ratio		1 : 1.4		Back Focal	Tele	16.4mm	
Max. Image Format		6.4mm x 4.8mm (φ8mm)		Length	Wide	11.0mm	
Operation Range	Iris	F1.4 - F16C		Flange Back Length		17.526mm	
	Focus	0.5m - Inf.		Mount		C-Mount	
	Zoom	4mm - 8mm		Filter Size		–	
Control	Iris	Manual		Dimensions		φ41.6mm x 48.8mm	
	Focus	Manual		Weight		72 g	
	Zoom	Manual					
Angle of View	D	1/2 type	115.9° - 58.8°	1/3 type	84.5° - 44.1°	1/4 type	62.7° - 33.1°
	H		90.4° - 47.0°		67.0° - 35.3°		50.0° - 26.5°
	V		67.0° - 35.3°		50.0° - 26.5°		37.4° - 19.8°
Operating Temperature		-20°C - +50°C					

Dimensions

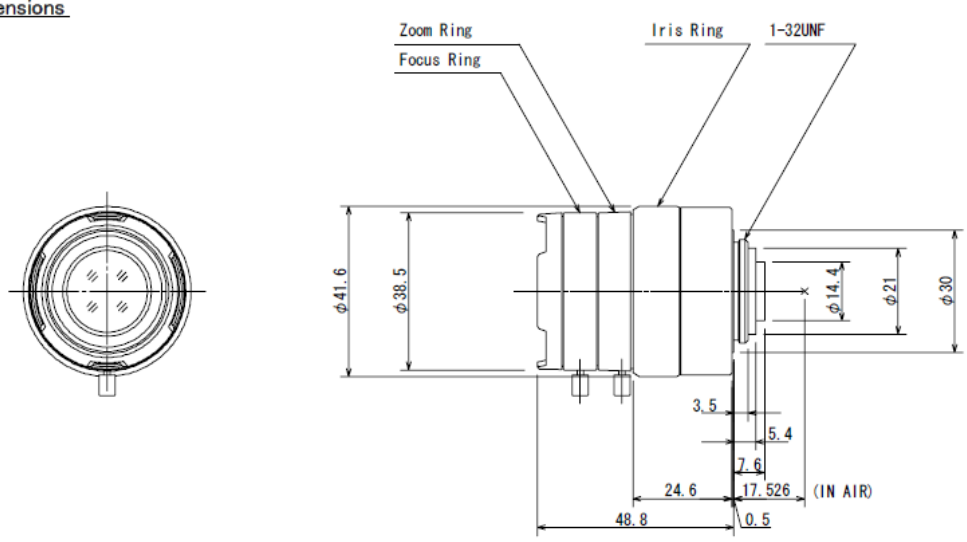

Specification is subject to change without any notice. 2006.7

Appendix C

Name: Dimethylsiloxane-bisphenol A-polycarbonate block co-polymer (MAX)

Purchased from: General Electric LR 3320, New Jersey, USA.

Solvent: Dichloromethane

Name: Poly(bisphenol A carbonate) (PBA) (Polycarbonate) Average M_w 64000 (GPC)

Purchased from: Aldrich Chemical Company, Inc. Milwaukee, WI 53233, USA.

Solvent: Dichloromethane

Name: Poly(butyl methacrylate-*co*-isobutyl methacrylate) (PBMA)

Purchased from: Aldrich Chemical Company, Inc. Milwaukee, WI 53233, USA.

Solvent: Dichloromethane

Name: Poly(methyl methacrylate) (PMMA)

Purchased from: Aldrich Chemical Company, Inc. Milwaukee, WI 53233, USA.

Solvent: Dichloromethane

Name: Poly(vinyl alcohol) (PVA) $M_{w:}$ 31000-50000

Purchased from: Sigma-Aldrich Co., St. Louis, MO 63103, USA

Solvent: Water (around 40-50 ^{o}C)

Name: Polystyrene Average M_w 45000

Purchased from: Aldrich Chemical Company, Inc. Milwaukee, WI 53233, USA.

Solvent: Dichloromethane

Name: Fluoroacrylic polymer (FIB)

Purchased from: ISSI, Dayton, OH, USA.

Solvent: Trifuorotoluene

Name: GP-533 silicone wax (Polysilicone)

Purchased from: Genesee Polymers Corporation, Burton, MI, USA

Solvent: Toluene

Solvent Name: Dichloromethane

Purchased from: EMD Chemicals Inc.

Solvent Name: Toluene

Purchased from: Fisher Scientific, Fair Lawn, NJ 07410, USA

Solvent Name: alpha,alpha,alpha-Trifluorotoluene (Trifluorotoluene)

Purchased from: ACROS Organics, NJ , USA

(Note: Toluene sometimes is added in Dichloromethane based solvent to slow the vaporization rate.)

Liquid Crystal Name: E-7

Purchased from: LCR HallCrest Inc

Liquid Crystal Name: NCU-192

Purchased from: LCR HallCrest Inc